Supplementary Information

for

Tandem fluorescent protein timers for *in vivo* analysis of protein dynamics

Anton Khmelinskii[1,2,7], Philipp J. Keller[2,3,7], Anna Bartosik[1,2,8], Matthias Meurer[1,2,8], Joseph D. Barry[4,8], Balca R. Mardin[1], Andreas Kaufmann[2,5], Susanne Trautmann[2,6], Malte Wachsmuth[2], Gislene Pereira[6], Wolfgang Huber[4], Elmar Schiebel[1#] and Michael Knop[1,2,6#]

[1] Zentrum für Molekulare Biologie der Universität Heidelberg, DKFZ-ZMBH Alliance; Im Neuenheimer Feld 282, D-69120 Heidelberg, Germany

[2] European Molecular Biology Laboratory (EMBL), Cell Biology and Biophysics Unit; Meyerhofstr. 1, D-69117 Heidelberg, Germany

[3] Janelia Farm Research Campus, Howard Hughes Medical Institute; 19700 Helix Drive, Ashburn, VA 20147, USA

[4] European Molecular Biology Laboratory (EMBL), Genome Biology Unit; Meyerhofstr. 1, D-69117 Heidelberg, Germany

[5] Present Address: ETH Zurich, Light Microscopy and Screening Center (LMSC); HPM F 16, Schafmattstr. 18, 8093 Zurich, Switzerland

[6] German Cancer Research Center, DKFZ-ZMBH Alliance; Im Neuenheimer Feld 581, D-69120 Heidelberg, Germany

[7, 8] These authors contributed equally to this work.

[#] Correspondence should be addressed to: M.K. (m.knop@zmbh.uni-heidelberg.de) and E.S. (e.schiebel@zmbh.uni-heidelberg.de).

This PDF file includes:

Nature Biotechnology: doi:10.1038/nbt.2281

Table of Contents

Nature Biotechnology: doi:10.1038/nbt.2281

1 Supplementary Methods

1.1 Measurement of FRET efficiency in the mCherry-sfGFP timer

FRET can occur from sfGFP to mCherry, but not in reverse, leading to a reduction in apparent molecular brightness of sfGFP. Consequently, the fluorescence intensity of sfGFP in the mCherry-sfGFP timer is reduced as a function of mCherry maturation. To determine the FRET efficiency (*E*) between sfGFP and mCherry, we compared the molecular brightness of sfGFP alone and in the mCherry-sfGFP fusion.

sfGFP and mCherry-sfGFP were expressed as N-terminally His-tagged fusions from plasmids pETM-11-6xHis-TEV-sfGFP (pMaM207) and pETM-11-6xHis-TEV-mCherry-sfGFP (pMaM208) in the *E. coli* strain BL21(DE3). Both recombinant proteins were affinity-purified using standard Ni-NTA purification, followed by cleavage of the His-Tag using recombinant TEV protease.

The recombinant proteins were diluted in yeast extract. Yeast extract was prepared by cell lysis with glass beads in lysis buffer (50 nM Tris pH 7.4, 150 mM NaCl, 0.01% NP-40 and protease inhibitors (cOmplete Ultra tablets (Roche) supplemented with 1 µg/ml Pepstatin)) and cleared by centrifugation (14000 rpm, 10 min).

The molecular brightness of sfGFP alone (CPM_{sfGFP}) and in the mCherry-sfGFP fusion ($CPM_{\text{mCherry-sfGFP}}$) and the fraction of mature/fluorescent mCherry were determined with fluorescence correlation spectroscopy (FCS). FCS measurements were conducted on a Leica SP5 confocal microscope (Leica) with sfGFP excitation at 488 nm wavelength (~7.5 kW·cm^{-2}) and emission at 505-550 nm, and mCherry excitation at 561 nm (~5.3 kW·cm^{-2}) and emission at 607-673 nm. Fluorescence fluctuation time-traces were acquired for 50 s and the auto- and cross-correlation curves were fitted with a 3D free diffusion model, with blinking and triplet terms. Blinking was treated as previously described[1]. A FRET efficiency of 0.173 ± 0.049 (mean ± s.d.) was determined using the equations detailed below. Similar results were obtained with recombinant proteins diluted in phosphate buffered saline (PBS, pH 7.4) (data not shown).

$$E = \frac{1 - \frac{CPM_{mCherry-sfGFP}}{CPM_{sfGFP}}}{q_{double}}$$

with

$$q_{double} = \frac{N_{sfGFP} \cdot CF_{green}}{N_{mCherry} \cdot CF_{red} \cdot CF_{volume}}$$

where *E* is the FRET efficiency,
CPM is the molecular brightness of sfGFP either alone or in the tandem FP fusion,
q_{double} is the fraction of mCherry-sfGFP fusions in which both sfGFP and mCherry are fluorescent,
N_{sfGFP} is the number of fluorescent sfGFP proteins in the detection volume (observed with the mCherry-sfGFP fusion),
$N_{mCherry}$ is the number of fluorescent mCherry proteins in the detection volume (observed with the mCherry-sfGFP fusion),
CF_{green} is the correction factor for background fluorescence of the solvent in the sfGFP channel detected with the same setting as the sample,
CF_{red} is the correction factor for background fluorescence of the solvent in the mCherry channel and cross talk from the sfGFP to the mCherry channel,
CF_{volume} is the volume size correction factor determined with Rhodamine Green excited at 488 nm and detected at 505-550 nm and at 607-673 nm.

Nature Biotechnology: doi:10.1038/nbt.2281

Average values of q_{double}, CPM_{sfGFP} and $CPM_{mCherry\text{-}sfGFP}$ were determined from five measurements of different dilutions of each recombinant protein.

1.2 Measurement of maturation kinetics of sfGFP and mCherry

The strain AK1212 expressing a non-degradable mCherry-sfGFP fusion under the control of the inducible *GAL1* promoter (*GAL1*^{pr}*-Ubi-M-RR-mCherry-sfGFP*, where RR indicates two lysine-to-arginine mutations in the degron) was grown at 30°C to OD_{600} 0.5-1.0 in SC-raffinose medium (synthetic complete medium with 3% w/v raffinose), diluted with fresh SC-raffinose medium and mixed at 10:1 ratio with wild type cells (ESM356-1) grown under the same conditions. 50 µl of the mixture were loaded into an observation chamber of a Y4C microfluidic plate (CellAsic), which was equilibrated at 30°C.

Before loading the cells, the observation chamber was washed for 3 min at 5 psi with water, treated for 20 min at 0.5 psi with a sterile-filtered solution of 2 mg/ml Concanavalin A (Sigma), washed again with water and flushed for 5 min at 5 psi with SC-raffinose medium. Cells were loaded into the observation chamber by applying a pressure of 5 psi for 10 s and washed for 5 min at 5 psi with SC-raffinose. Imaging of ten different fields of view was started after switching to a constant flow at 1 psi. Bright field, sfGFP and mCherry images were acquired every 3 min on a DeltaVision RT microscope (Applied Precision) equipped with a 60x/1.40 NA Plan Apo oil objective (Olympus), a CoolSNAP HQ camera (Photometrics), appropriate filters and a custom-built incubator box set to 30°C. After acquisition of the first time point, the medium was switched to SC-raffinose/galactose (synthetic complete medium with 3% raffinose and 2% galactose) to induce transcription of the non-degradable mCherry-sfGFP fusion. Additionally, images from observation chambers containing only medium (for background correction) and images from observation chambers containing Alexa488 and Alexa594 dye solutions or only water (for flat field correction) were acquired. Image correction, segmentation and quantification of mCherry and sfGFP fluorescence intensities of single cells over time were done with custom software written in MATLAB (MathWorks).

Maturation rate constants of sfGFP and mCherry were determined from the induction time course data in two steps (Supplementary Fig. 8a). First, mCherry intensity curves were fitted using a two-step maturation model (E26 in Section 3.4). mCherry maturation rate constants and induction time point were assigned as open parameters, whereas the degradation rate constant of the non-degradable mCherry-sfGFP fusion was determined according to E37 (Section 3.6) from the population doubling time T_{cycle} = 136 min measured in the induction time-lapse series and assuming an infinite half-life of the fusion. In the second step, sfGFP intensity curves were fitted using a one-step maturation model with FRET (E27 in Section 3.4). sfGFP maturation rate constant and induction time point were assigned as open parameters, whereas the degradation rate constant was set as before in the mCherry fit, the FRET efficiency was set to 0.173 (determined in Section 1.1), and mCherry maturation rate constants were set to the parameters resulting from mCherry fitting.

Maturation rate constants were calculated independently for each cell. Subsequently, final maturation rate constants were determined as medians values (n = 35), considering only the sub-population of cells yielding a better than median χ^2 value in model fitting. The obtained maturation half-times are: T_1 = 16.91 ± 1.23 min, T_2 = 30.30 ± 1.88 min for mCherry and T = 5.63 ± 0.82 min for sfGFP (median ± s.e.m.) (Supplementary Fig. 8a).

Nature Biotechnology: doi:10.1038/nbt.2281

2 Supplementary Text

2.1 Supplementary Note 1

Comparison between conventional FTs and tandem FP timers

To demonstrate that tandem FP fusions can function as FTs, we compared the behavior of a conventional FT (Fast-FT[2]) with the mCherry-sfGFP fusion. The maturation curves of Fast-FT and mCherry-sfGFP were calculated for fixed populations of molecules (in the first non-fluorescent state at time zero), as described in Section 3.7. This analysis shows that the mCherry-sfGFP fusion is a timer since the mCherry/sfGFP intensity ratio provides a measure of protein age (Fig. 1).

Figure 1 also reveals important differences between conventional FTs and tFTs. The red/blue intensity ratio of Fast-FT continues to increase as the protein pool ages. In contrast, the mCherry/sfGFP intensity ratio reaches a plateau once the maturation of mCherry molecules is nearly complete. This would suggest that processes in a wider range of time scales could be studied with conventional FTs. In practice, however, the dynamic range of conventional FTs is limited. First, the population of molecules in the first fluorescent state (FT blue form in Fig. 1a) gradually disappears as conventional FTs mature, leading to a decrease in the signal-to-noise ratio of fluorescence intensity measurements. On the contrary, the signal-to-noise ratio increases as tFTs mature. In addition, the fast maturation of sfGFP allows fluorescence detection shorty after synthesis of mCherry-sfGFP fusions (Fig. 1b). Second, existing conventional FTs are considerably dimmer than mCherry or sfGFP (the intensity curves in Fig. 1 are all normalized to the brightness of sfGFP). Although intracellular trafficking of overexpressed protein fusions could be followed with monomeric FTs[2], yeast nucleoporins tagged endogenously with Fast-FT are not detectable with fluorescence microscopy (data not shown). Together, these properties make tFTs highly suitable for studies of protein degradation kinetics (especially if protein fusions are expressed at endogenous levels), although analysis of protein turnover is theoretically possible with conventional FTs (see Section 3.5).

2.2 Supplementary Note 2

Single-cell analysis with tFTs

tFTs can be used to estimate the relative age of distinct intracellular protein pools. The analysis of *SPC42-mCherry-sfGFP* and *RAX2-mCherry-sfGFP* cells indicates that comparative measurements with the mCherry-sfGFP timer are robust within single cells as the relative age of different structures was determined accurately in nearly every individual cell (Fig. 2). However, significant cell-to-cell variation in the $\boldsymbol{R}_b/\boldsymbol{R}_m$ or the absolute mCherry/sfGFP ratios of similar structures is apparent. Different factors contribute to this variability.

First, fluorophore maturation in any FP is a stochastic process. It is therefore important to stress that tFTs cannot be used to determine the age of single molecules. Significant cell-to-cell variability in $\boldsymbol{R}$ values is expected for cellular structures with low number of tFT-tagged molecules.

Second, the cell history should be considered when evaluating structures with age-dependent partitioning. In the experiment with SPBs marked with Spc42-mCherry-sfGFP (Fig. 2a-c), cell-to-cell variability in $\boldsymbol{R}_b/\boldsymbol{R}_m$ ratios of SPBs is largely explained by the fact that old SPBs are inherited from one bud to the next. Therefore, the age of the old SPB varies between cells – half of the population has one-generation old SPBs, a quarter of the population has two-generations old SPBs, etc. – and the age difference between the new and the old SPBs in dividing cells varies accordingly. In the analysis of structures marked with Rax2-mCherry-sfGFP (Fig. 2e, f), cells within the same stage class differ in age by as much as 30 min. Furthermore, there are differences in cell cycle duration between individual

Nature Biotechnology: doi:10.1038/nbt.2281

cells. Together, these factors contribute to the observed variability of mCherry/sfGFP intensity ratios.

Differences in protein degradation kinetics between individual cells could constitute another source of variability. tFTs could therefore provide an opportunity to measure the contribution of protein degradation to the biological noise in protein abundance[3]. Finally, cell-to-cell variability in physicochemical properties of the intracellular environment, which could affect the maturation and brightness of fluorescent proteins, cannot be excluded.

2.3 Supplementary Note 3

Nucleoporin exchange between nuclear envelope and cytoplasm

During mitosis in *S. cerevisiae* the nuclear envelope does not break down and NPCs remain intact, in contrast to organisms with open mitosis. In the absence of assembly of new NPCs, existing NPCs are partitioned between mother and bud nuclear envelopes during nuclear division[4,5]. This observation indicates that NPCs are stable structures and their subunits (at least the scaffold nucleoporins) do not shuttle between assembled NPCs and cytoplasmic pools.

We formulated the rate equations describing turnover and dynamics of nucleoporins tagged with the mCherry-sfGFP timer (Section 3.8). We considered that nucleoporin production occurs at a constant rate p in the cytoplasm. Fusions in any maturation state are transferred at a constant rate a from the cytoplasm to the nuclear envelope (but not in the opposite direction, as NPCs are stable). Nucleoporin degradation occurs in both pools, but with different rate constants k_1 and k_2. Using the kinetic parameters of the mCherry-sfGFP timer determined in this study (Sections 1.1 and 1.2, Supplementary Fig. 8a), we demonstrate that the steady-state mCherry/sfGFP intensity ratio is expected to be always higher at the nuclear envelope than in the cytoplasm if NPCs are stable structures (Section 3.8).

Our analysis of nucleoporins tagged with mCherry-sfGFP in *S. cerevisiae* confirmed this expectation, especially for scaffold components of the NPC such as outer and inner ring nucleoporins (Fig. 3a, b). This experiment illustrates how the mCherry-sfGFP timer can be applied to investigate intracellular protein mobility, in addition to the analysis of protein inheritance (Fig. 2) and turnover (Fig. 4).

2.4 Supplementary Note 4

Analysis of protein degradation kinetics with tandem FP timers

A tandem FP fusion functions as an FT if the two fluorophores in the pair mature with different kinetics. The ratio of fluorescent intensities measured for a protein tagged with a tandem FP timer depends on the kinetics of protein turnover and mobility in the cell and on the properties of the timer.

For mCherry-sfGFP fusions in steady state, the mCherry/sfGFP intensity ratio depends on the degradation rate constant k of the fusion but is independent of the protein production rate p, as we demonstrate experimentally with Ubi-**X**-mCherry-sfGFP constructs (Fig. 4).

This relationship can be proved by formulating the rate equations of protein turnover, as detailed in the following sections. If mCherry and sfGFP are fused, they are subject to the same production and degradation rate constants p and k. Considering that sfGFP matures in a one-step process with maturation rate constant m (see Section 3.1) and mCherry undergoes a two-step maturation with maturation rate constants m_1 and m_2 (see Section 3.2), the steady-state ratio Γ of the respective fluorescent populations $\bar{N}_{m,mCherry}$ and $\bar{N}_{m,sfGFP}$ is given by:

Nature Biotechnology: doi:10.1038/nbt.2281

$$\Gamma = \frac{\bar{N}_{m,mCherry}}{\bar{N}_{m,sfGFP}} = \frac{m_1 m_2 \left(k + m\right)}{m\left(k + m_1\right)\left(k + m_2\right)}$$ E1 (E16 derived in Section 3.3)

Importantly, the emission spectrum of sfGFP significantly overlaps with the excitation spectrum of mCherry. This can result in FRET (Förster Resonance Energy Transfer[6]), whereby excitation of sfGFP leads to emission by mCherry instead of sfGFP. Taking this effect into consideration (see Section 3.4), the mCherry/sfGFP ratio of fluorescence intensities $\tilde{R}$ is given by:

$$\tilde{R} = \frac{I_{mCherry}}{\tilde{I}_{sfGFP}} = f\frac{m_1 m_2 \left(k + m\right)}{m\left(k\left(k + m_1 + m_2\right) + m_1 m_2 \left(1 - E\right)\right)}$$ E2 (E25 derived in Section 3.4)

E2 demonstrates that the mCherry/sfGFP intensity ratio depends on *k* but is independent of *p*, as observed with Ubi-**X**-mCherry-sfGFP constructs (Fig. 4).

The mCherry-sfGFP timer provides a dynamic range suitable for systematic analysis of protein degradation kinetics in *S. cerevisiae* (Supplementary Fig. 8b, c), considering that the average half-life of the yeast proteome is ~43 min[7] and the population doubling time is typically between 90 and 120 min.

2.5 Supplementary Note 5

Influence of tFTs on protein function and turnover

The potential impact of a tag on the function and turnover of tagged proteins should be considered both in single protein and proteome-wide studies. A tag can influence protein turnover by promoting protein aggregation, adding dominant degradation signals, masking degradation signals, impairing correct protein folding or preventing correct protein localization and/or assembly into complexes.

When using tFTs as protein tags, care has to be taken to ensure that such tandem FP fusions contain only truly monomeric FPs. For example, tandem fusions of early GFP variants, which have a weak tendency to dimerize, can lead to aggregation of otherwise soluble proteins. We routinely use Fus3 to evaluate FP-mediated protein oligomerization in *S. cerevisiae*. Fus3 is appears to be very sensitive to aggregation triggered by sticky FPs. Tagging of Fus3 with conventional FPs like Citrine or three tandem copies of a widely used EGFP (Clontech) leads to formation of a perinuclear aggregate. No aggregates were observed in cells expressing Fus3-mCherry-sfGFP (data not shown).

A protein tag can contain signals that target any protein fusion for degradation. Cells expressing mCherry-sfGFP have a very high mCherry/sfGFP intensity ratio, indicating that the mCherry-sfGFP timer is intrinsically stable. Nevertheless, folding of mCherry-sfGFP may be impaired in particular cases, which then could affect the stability of the tagged protein.

The large size of tFTs compared to common epitope tags or single FPs could exacerbate the negative effects of tagging related to steric hindrance, e.g. protein mislocalization. In our experience, doubling the tag size from a single FP to a tFT does not cause systematic problems. For instance, out of 960 essential yeast genes that could be endogenously tagged with mCherry, 958 could also be tagged with mCherry-sfGFP without obvious impact on cell growth (A. Khmelinskii, M. Meurer and M. Knop, unpublished data). This suggests that the

Nature Biotechnology: doi:10.1038/nbt.2281

turnover of most proteins successfully tagged with GFP and TAP tag in earlier proteome-wide studies[8,9] could be analyzed with tFTs.

Finally, the position of the tag should be considered. C-terminal, N-terminal and internal protein tagging can all influence protein turnover. In particular cases the effect of a tag could be determined by comparing the behavior of fusions with different tag locations.

C-terminal tagging – The experiments conducted in this study used synthetic constructs and endogenous yeast proteins tagged with mCherry-sfGFP mostly at the C-terminus. Although a tag can influence the marked protein, C-terminal tagging appears to have the lowest likelihood of interfering with protein function and ~84% of essential proteins (total of 1034 essential proteins) in *S. cerevisiae* can accommodate a tag at the C-terminus[8,9].

Internal tagging – Proteins in *S. cerevisiae* can be tagged internally using a two-step procedure[10]. However, many positions in a protein are sensitive to insertions, which could affect protein folding and possibly protein stability, localization and function. Hence, attempts to tag a protein internally require careful consideration of the insertion point and subsequent validation of protein functionality.

N-terminal tagging – Recent evidence suggests that the first residues of many proteins carry potential N-terminal degradation signals[11]. This does not preclude the application of tFTs for N-terminal tagging of select proteins (e.g. Prm3 (Fig. 3c) was tagged at the N-terminus), but is likely to bring additional uncertainties to genome-wide protein turnover studies.

2.6 Supplementary Note 6

Systematic identification of N-end rule pathway components

We used strains expressing Ubi-**X**-mCherry-sfGFP fusions with destabilizing motifs recognized by different branches of the N-end rule to systematically screen for components of this pathway (Fig. 5a, b). Though commonly used, Ubi-**X**-protein fusions are not perfect reporters of N-end rule pathway activity as proteolytic removal of ubiquitin is required to unmask the N-degrons before they can be recognized by the *UBR1* or *DOA10* pathways. For this reason, we performed also a control screen was conducted with a strain expressing mCherry-sfGFP with a ubiquitin moiety at the N-terminus. As the impact of each gene deletion on a particular Ubi-**X**-mCherry-sfGFP fusion is compared to its impact on the control fusion (see Online Methods), ubiquitin proteases should not be identified as factors involved in degradation of Ubi-**X**-mCherry-sfGFP fusions.

The control screen was also instrumental in eliminating false-positives as the behavior of all mCherry-sfGFP fusions was strongly affected in a large set of gene deletion strains. This set of genes was highly enriched in genes with mitochondrial functions (Supplementary Fig. 12), suggesting that the intracellular environment of cells with defective mitochondria affects the brightness and/or the maturation of the mCherry-sfGFP timer.

Practically all known components of the *UBR1* and *DOA10* branches of the N-end rule pathway were reproducibly identified in the genome-wide screens conducted in this study (Fig. 5, Supplementary Fig. 13). The few exceptions were:

*ubc6*Δ (expected to stabilize Ubi-CL-mCherry-sfGFP) – absent from the library;

*ufd1*Δ (expected to stabilize Ubi-P-mCherry-sfGFP) – strains deleted for *UFD1* are not viable and thus could not be analyzed.

Ubi-N-mCherry-sfGFP and Ubi-Q-mCherry-sfGFP fusions were apparently stabilized by deletion of *SCS22* (Fig. 5f), which encodes a protein linked to regulation of phospholipid biosynthesis[12]. However, this stabilization could not be confirmed in an independently generated *scs22Δ* strain (data not shown). Genetic analysis of the library strain revealed that an additional mutation not linked to *scs22*Δ caused the observed stabilization. Since only the

Nature Biotechnology: doi:10.1038/nbt.2281

Ubi-N/Q-mCherry-sfGFP fusions were stabilized, the mutation is likely to affect the *NTA1* or *ATE1* genes.

In addition to pathway-specific factors, general components of the ubiquitin-proteasome system or factors regulating the expression, localization, turnover and activity of the degradation machinery can be identified in the screens. Indeed, deletions of genes encoding various proteasomal subunits (*PRE9*, *SEM1*, *RPN9*, *RPN10*), factors involved in expression (*UFD5*/*RPN4*) and assembly (*IRC25*, *POC4*, *UMP1*) of proteasomal subunits, factors involved in ubiquitin homeostasis (*BRO1*, *DOA4*, *HUL5*, *UBP6*, *UFD3*/*DOA1*) and ubiquitin itself (*UBI4*) were observed to stabilize different Ubi-**X**-mCherry-sfGFP fusions (Fig. 5f, Supplementary Figs. 13 and 14). The indirect role of some of these factors in degradation of Ubi-**X**-mCherry-sfGFP fusions is suggested by the weak stabilization observed in the corresponding deletion strains.

Nature Biotechnology: doi:10.1038/nbt.2281

3 Supplementary Theory

3.1 Turnover of GFP-like fluorescent proteins (one-step maturation)

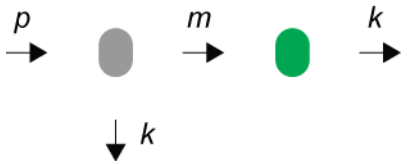

In this model, we assume that an FP is produced at a constant rate *p* as a non-fluorescent protein, matures to a fluorescent protein in a single step with the maturation rate constant *m* and is degraded with the rate constant *k*. Degradation occurs for both non-mature and mature proteins, i.e. the early non-fluorescent translation products as well as the fully matured FPs.

As a result of the one-step maturation process, there are two populations of FP species: a non-fluorescent population with N_d members and a fluorescent population with N_m members that results by maturation of members of the first population. The following rate equations describe the dynamics of N_d and N_m:

$$dN_d = pdt - mN_d dt - kN_d dt \quad \text{E3}$$

$$dN_m = mN_d dt - kN_m dt \quad \text{E4}$$

The steady-state solution of the set of differential equations E3-E4 is as follows:

$$\bar{N}_d = \frac{p}{k+m} \quad \text{E5}$$

$$\bar{N}_m = \frac{pm}{k(k+m)} \quad \text{E6}$$

Assuming population sizes of zero for both N_d and N_m at time zero, the time-dependent solution for the mature population N_m defined by the set of differential equations E3-E4 is:

$$N_m(t) = \frac{p}{k+m}\left(\frac{m}{k} + \exp\{-(k+m)t\}\right) - \frac{p}{k}\exp\{-kt\} \quad \text{E7}$$

3.2 Turnover of mCherry-like fluorescent proteins (two-step maturation)

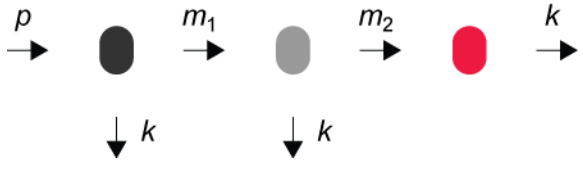

The one-step maturation model is based on the assumption that switching from the non-mature to the mature state of a fluorophore requires only a single kinetic step. Consequently, a single rate constant *m* is required to describe the kinetic transition. In contrast, the two-step maturation model considers an initial transition to an intermediate state before arriving

Nature Biotechnology: doi:10.1038/nbt.2281

at the mature fluorophore in a second kinetic transition. The maturation rate constants m_1 and m_2 characterize the transitions from the non-mature population N_d to the intermediate population N_i and from the intermediate population N_i to the mature population N_m, respectively. The following set of differential equations describes the kinetics in this model:

$$dN_d = pdt - m_1 N_d dt - kN_d dt \quad \text{E8}$$

$$dN_i = m_1 N_d dt - m_2 N_i dt - kN_i dt \quad \text{E9}$$

$$dN_m = m_2 N_i dt - kN_m dt \quad \text{E10}$$

The steady-state solution of the set of differential equations E8-E10 is as follows:

$$\bar{N}_d = \frac{p}{k + m_1} \quad \text{E11}$$

$$\bar{N}_i = \frac{pm_1}{\left(k + m_1\right)\left(k + m_2\right)} \quad \text{E12}$$

$$\bar{N}_m = \frac{pm_1 m_2}{k\left(k + m_1\right)\left(k + m_2\right)} \quad \text{E13}$$

Assuming population sizes of zero for N_d, N_i and N_m at time zero, the time-dependent solution for the mature population N_m defined by the set of differential equations E8-E10 is given by:

$$N_m\left(t\right) = \frac{p}{k}\left(\frac{m_1 m_2}{\left(k + m_1\right)\left(k + m_2\right)} - \exp\left\{-kt\right\}\right) + \frac{p}{m_1 - m_2}\left(\frac{m_1}{k + m_2}\exp\left\{-\left(k + m_2\right)t\right\} - \frac{m_2}{k + m_1}\exp\left\{-\left(k + m_1\right)t\right\}\right) \quad \text{E14}$$

In the special case $m_1 = m_2 = m$, E14 can be reduced to:

$$N_m\left(t\right) = \frac{p}{k + m}\left(\frac{m^2}{k\left(k + m\right)} + \left(\frac{m}{k + m} + \left(mt + 1\right)\right)\exp\left\{-\left(k + m\right)t\right\}\right) - \frac{p}{k}\exp\left\{-kt\right\} \quad \text{E15}$$

3.3 Turnover of the mCherry-sfGFP timer without FRET

Tandem FP timers are formed by fusion of two FPs with distinct kinetics of fluorophore maturation. If two FPs A and B, present in the same polypeptide and therefore degraded with the same degradation rate constant *k*, are considered such that A undergoes a two-step maturation with rate constants m_1 and m_2 and B matures in a one-step process with the maturation rate constant *m*, the steady-state ratio Γ of the respective fluorescent populations $\bar{N}_{m,A}$ and $\bar{N}_{m,B}$ (obtained in E13 and E6) is given by:

Nature Biotechnology: doi:10.1038/nbt.2281

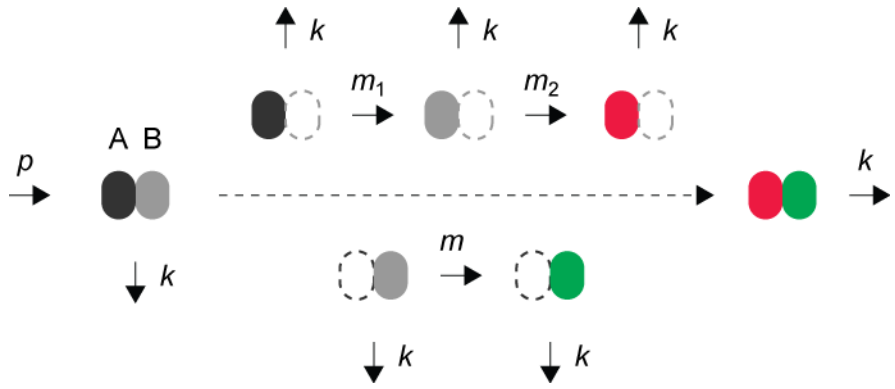

$$\Gamma = \frac{\bar{N}_{m,A}}{\bar{N}_{m,B}} = \frac{m_1 m_2 \left(k+m\right)}{m\left(k+m_1\right)\left(k+m_2\right)} \qquad \text{E16}$$

Thus, whereas the total amount of fluorescent species in steady state is dependent on the protein production rate *p*, the ratio of fluorescence observed for tandem FP fusions is independent of *p*. The ratio R of the fluorescence intensities I_A and I_B of the two fluorescent populations is proportional to the steady-state ratio Γ, where f is the proportionality constant specific to each system for fluorescence intensity measurements:

$$R = \frac{I_A}{I_B} = f\Gamma = f\frac{\bar{N}_{m,A}}{\bar{N}_{m,B}} \qquad \text{E17}$$

Whereas sfGFP appears to mature according to a one-step kinetic model, our data also indicate that the two-step maturation model describes mCherry maturation better than the one-step model (Supplementary Fig. 8a). We therefore suggest introducing a maturation rate constant *m* according to E6 for sfGFP maturation and maturation rate constants m_1 and m_2 according to E13 to describe mCherry maturation. Combining equations E6 with E13 provides an analytical description of the fluorescence intensity ratio R measured for mCherry-sfGFP fusions in steady state:

$$R = \frac{I_{mCherry}}{I_{GFP}} = f\frac{m_1 m_2 \left(k+m\right)}{m\left(k+m_1\right)\left(k+m_2\right)} \qquad \text{E18}$$

This description is only accurate if no FRET (Förster Resonance Energy Transfer[6]) occurs between sfGFP and mCherry in the timer (see below).

3.4 Turnover of the mCherry-sfGFP timer with FRET

In a tandem FP fusion, excitation of one fluorophore may result in fluorescence emission by the second fluorophore rather than by the fluorophore that initially absorbed the photon. This phenomenon, termed FRET, can occur if the excitation spectrum of the acceptor fluorophore A (e.g. mCherry) overlaps significantly with the emission spectrum of the donor fluorophore B (e.g. sfGFP) and if the spatial distance between the two fluorophores is sufficiently small. The FRET efficiency *E* is then defined as the probability by which the energy absorbed by the fluorophore B is transferred to the fluorophore A. In the event of such an energy transfer,

Nature Biotechnology: doi:10.1038/nbt.2281

the fluorophore B will not emit fluorescence. Consequently, the fluorescence intensity signal measured for the population of type B will underestimate the population count of mature fluorophores of type B if FRET is not considered in the data analysis.

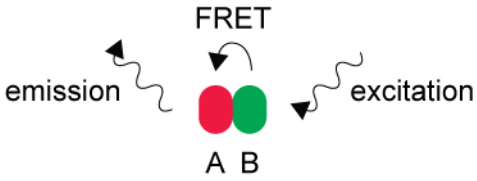

In the following, we detail the influence of FRET on the measurement of fluorescence intensity ratios of tandem FP fusions. We assume that FRET is possible from fluorophore B to fluorophore A but not from fluorophore A to fluorophore B. The fluorescence intensity I_A measured by using an excitation wavelength that only allows direct excitation of fluorophores of type A is FRET-independent and proportional to the number $\bar{N}_{m,A}$ of mature A fluorophores:

$$I_A = f_A \bar{N}_{m,A} \qquad \text{E19}$$

In contrast, the FRET-dependent fluorescence intensity $\tilde{I}_B$ of the population of fluorophores of type B results from tandem FP fusions in two distinct states. The first state is not affected by FRET and characterized by a mature fluorophore of type B that is combined with a non-mature fluorophore of type A. In the second state, exhibiting reduced type B fluorescence due to FRET, a mature fluorophore of type B is combined with a mature fluorophore of type A. In this latter configuration, a portion *E* of the overall excitation energy will be transferred from type B to type A fluorophores and thus, the type B intensity signal will be reduced accordingly. The FRET-dependent intensity $\tilde{I}_B$ measured from the population of fluorophores of type B upon light excitation is proportional to the number $\bar{N}_{m,B}$ of mature fluorophores of type B and a multiplicative term that is influenced by the FRET efficiency *E*. By defining *b* as the steady-state probability for a neighbor of a mature type B fluorophore being a mature type A fluorophore, $\tilde{I}_B$ can be expressed as follows:

$$\tilde{I}_B = f_B \bar{N}_{m,B} \left(\left(1-b\right) + b\left(1-E\right) \right) \qquad \text{E20}$$

By substituting the instrument-specific proportionality constant $f = f_A / f_B$ introduced above (Section 3.3), the FRET-dependent intensity ratio $\tilde{R}$ then results as:

$$\tilde{R} = \frac{I_A}{\tilde{I}_B} = f \frac{\bar{N}_{m,A}}{\bar{N}_{m,B} \left(\left(1-b\right) + b\left(1-E\right) \right)} = f\Gamma \frac{1}{\left(1-bE\right)} \qquad \text{E21}$$

We now specifically consider a tandem FP fusion that consists of a two-step maturing fluorophore of type A and a one-step maturing fluorophore of type B. The mCherry-sfGFP timer used in our study is representative of this scenario.

Nature Biotechnology: doi:10.1038/nbt.2281

According to E19, the FRET-independent intensity I_A measured from the population of fluorophores of type A upon light excitation at the respective excitation wavelength is proportional to $\bar{N}_{m,A}$ as defined in E13:

$$I_A = f_A \frac{p m_1 m_2}{k\left(k+m_1\right)\left(k+m_2\right)} \qquad \text{E22}$$

The steady-state probability b for a neighbor of a mature fluorophore of type B being a mature fluorophore of type A can be calculated from E11-E13:

$$b = \frac{\bar{N}_{m,A}}{\bar{N}_{d,A} + \bar{N}_{i,A} + \bar{N}_{m,A}} = \frac{m_1 m_2}{\left(k+m_1\right)\left(k+m_2\right)} \qquad \text{E23}$$

Thus, the FRET-dependent intensity $\tilde{I}_B$ defined in E20 results as:

$$\tilde{I}_B = f_B \frac{pm}{k\left(k+m\right)} \frac{k(k+m_1+m_2)+m_1 m_2(1-E)}{\left(k+m_1\right)\left(k+m_2\right)} \qquad \text{E24}$$

Finally, we obtain the FRET-dependent intensity ratio $\tilde{R}$:

$$\tilde{R} = \frac{I_A}{\tilde{I}_B} = f \frac{m_1 m_2\left(k+m\right)}{m\left(k\left(k+m_1+m_2\right)+m_1 m_2\left(1-E\right)\right)} = f\tilde{\Gamma} \qquad \text{E25}$$

The absence of FRET is defined by the special case $E = 0$, in which E25 can be reduced to the FRET-independent intensity ratio R defined in E18.

Assuming population sizes of zero for $N_{d,A}$, $N_{i,A}$, $N_{m,A}$, $N_{d,B}$ and $N_{m,B}$ at time zero, the time-dependent solution for the FRET-independent intensity I_A is proportional to $N_{m,A}(t)$ as defined in E14:

$$\begin{aligned} I_A(t) = {} & f_A \frac{p}{k}\left(\frac{m_1 m_2}{\left(k+m_1\right)\left(k+m_2\right)} - \exp\{-kt\}\right) \\ & + f_A \frac{p}{m_1 - m_2}\left(\frac{m_1}{k+m_2}\exp\{-\left(k+m_2\right)t\} - \frac{m_2}{k+m_1}\exp\{-\left(k+m_1\right)t\}\right) \end{aligned} \qquad \text{E26}$$

The FRET-dependent intensity $\tilde{I}_B$ is given by:

Nature Biotechnology: doi:10.1038/nbt.2281

$$\tilde{I}_B(t) = f_b\left(\frac{p}{k+m}\left(\frac{m}{k}+\exp\{-(k+m)t\}\right)-\frac{p}{k}\exp\{-kt\}\right) \cdot\left(1-\frac{N_{m,A}(t)}{N_{d,A}(t)+N_{i,A}(t)+N_{m,A}(t)}E\right) \quad \text{E27}$$

with $N_{m,A}(t)$ as defined in E14 and:

$$N_{d,A}(t) = \frac{p}{(k+m_1)}\left(1-\exp\{-(k \quad m_1)t\}\right) \quad \text{E28}$$

$$N_{i,A}(t) = \frac{pm_1}{(k+m_1)(k+m_2)(m_1 \quad m_2)} \cdot\left((m_1-m_2)-(k+m_1)\exp\{-(k+m_2)t\}+(k+m_2)\exp\{-(k \quad m_1)t\}\right) \quad \text{E29}$$

3.5 Turnover of conventional FTs

In this model we consider the turnover of conventional FTs using the three-step maturation model (C→B→I→R, detailed in Ref.[13]), with non-fluorescent states C and I, a blue-fluorescent state B and a red-fluorescent state R. An FT molecule in each state undergoes a one-step conversion into the next state with rate constant m_b, m_i and m_r, respectively. Assuming constant production of FT molecules in state C (rate constant p) and degradation of FT molecules in all maturation states with the same rate constant k, the turnover of a conventional FT is described by the set of differential equations E30-E33:

$$dC = pdt-(m_b+k)Cdt \quad \text{E30}$$

$$dB = m_bCdt-(m_i+k)Bdt \quad \text{E31}$$

$$dI = m_iBdt-(m_r+k)Idt \quad \text{E32}$$

$$dR = m_rIdt-kRdt \quad \text{E33}$$

The steady-state population sizes $\bar{B}$ and $\bar{R}$ result as:

$$\bar{B} = \frac{pm_b}{(k+m_b)(k+m_i)} \quad \text{E34}$$

$$\bar{R} = \frac{pm_bm_im_r}{k(k+m_b)(k+m_i)(k+m_r)} \quad \text{E35}$$

Consequently, the steady-state ratio $\bar{R}/\bar{B}$ is independent of the protein production rate p:

$$\frac{\bar{R}}{\bar{B}} = \frac{m_im_r}{k(k+m_r)} \quad \text{E36}$$

Nature Biotechnology: doi:10.1038/nbt.2281

This result indicates that a conventional FT reports on the kinetics of protein degradation in steady state, similarly to tandem FP timers.

3.6 Protein degradation and dilution

The turnover models detailed above (Sections 3.1-3.5) demonstrate how ratiometric fluorescence measurements with tandem FP timers relate to kinetics of protein degradation. Importantly, two distinct processes contribute to protein degradation in the cell: effective protein degradation (destruction) and protein removal due to cell division (dilution). Thus, the degradation rate constant *k* used in the maturation models can be decomposed into two terms:

$$k = k_{deg} + k_{cycle} \qquad \text{E37}$$

where k_{deg} is the rate constant of effective protein degradation, related to the protein half-life T_{deg}, defined as $T_{deg} = \ln(2)/k_{deg}$, and k_{cycle} is the dilution rate constant, related to the cell cycle duration $T_{cycle} = \ln(2)/k_{cycle}$.

Combining E37 with E25 indicates that ratiometric fluorescence measurements with tandem FP timers are affected by cell cycle duration. Direct comparison of different proteins tagged with a tandem FP timer requires all cells to be grown under strictly identical conditions.

3.7 Maturation of conventional FTs and tandem FP timers

The time-course of Fast-FT maturation (Fig. 1a) was calculated using a three-step kinetic model (C→B→I→R, detailed in Section 3.5). The per-hour transition rates are given by Subach *et al.* (Ref.[2]) as $m_b = 8.7$, $m_i = 0.78$ and $m_r = 0.14$. Assuming zero population sizes at time point zero, the time-dependent population fractions $B(t)$ and $R(t)$ result as:

$$B(t) = \frac{m_b}{m_b - m_i}\left(\exp\{-m_i t\} - \exp\{-m_b t\}\right) \qquad \text{E38}$$

$$\begin{aligned} R(t) = \frac{1}{(m_b - m_i)(m_b - m_r)(m_i - m_r)}\Big(& m_i m_r \left(m_i - m_r\right)\left(1 - \exp\{-m_b t\}\right) \\ & + m_b^2 \left(m_i\left(1 - \exp\{-m_r t\}\right) - m_r\left(1 - \exp\{-m_i t\}\right)\right) \\ & + m_b \left(m_r^2\left(1 - \exp\{-m_i t\}\right) - m_i^2\left(1 - \exp\{-m_r t\}\right)\right)\Big) \end{aligned} \qquad \text{E39}$$

For the mCherry-sfGFP fusion (Fig. 1b), the time-dependent fractions of the green-fluorescent $G(t)$ and red-fluorescent $C(t)$ populations were calculated using a one-step kinetic model for sfGFP and a two-step kinetic model for mCherry as follows:

$$G(t) = 1 - \exp\{-mt\} \qquad \text{E40}$$

Nature Biotechnology: doi:10.1038/nbt.2281

$$C(t) = \frac{m_1\left(1-\exp\{-m_2 t\}\right) - m_2\left(1-\exp\{-m_1 t\}\right)}{m_1 - m_2} \qquad \text{E41}$$

The maturation rate constants of sfGFP (m) and mCherry (m_1 and m_2) determined in this study (Section 1.2) were used for the calculation.

Normalized time-dependent intensity levels were calculated from the time-dependent population fractions, using published quantum efficiencies and extinction coefficients of each FP: quantum efficiencies of 0.3 for the blue form of Fast-FT, 0.09 for the red form of Fast-FT, 0.65 for sfGFP and 0.22 for mCherry; extinction coefficients of 49700 $M^{-1}cm^{-1}$ for the blue form of Fast-FT, 75300 $M^{-1}cm^{-1}$ for the red form of Fast-FT, 83300 $M^{-1}cm^{-1}$ for sfGFP and 72000 $M^{-1}cm^{-1}$ for mCherry[2,14,15]. All intensity curves were normalized to that of sfGFP. Following normalization, sfGFP intensity levels were additionally corrected for FRET, using the FRET efficiency of 0.173 determined for the mCherry-sfGFP fusion in this study (Section 1.1).

Additionally, we examined the impact of fluorophore maturation kinetics on the dynamic range of tandem FP fusions. For that purpose we compared the dynamic range of different tandem FP timers by keeping one FP constant and varying the second FP (Supplementary Fig. 1). All intensity curves were calculated as detailed for the mCherry-sfGFP fusion without the FRET correction. The intensity ratio curves were normalized to the maximum in each plot. The maturation kinetics of mOrange and DsRed1 (Supplementary Fig. 1a) were described by a two-step kinetic model according to E41, with published maturation half-times divided by two for each maturation transition[15]. The maturation kinetics of theoretical FPs GFPslow1 and GFPslow2 (Supplementary Fig. 1b) were described by a one-step kinetic model according to E40, with maturation half-times of 45 min (GFPslow1, maturation rate similar to mCherry) and 2.5 h (GFPslow2, maturation rate similar to mOrange).

3.8 Turnover and mobility of nucleoporins (two-compartment model)

We extended the model of mCherry-sfGFP turnover (Section 3.4) to incorporate two intracellular compartments (pool 1 – e.g. cytoplasm, pool 2 – e.g. nuclear envelope). In this scenario, protein production occurs at a constant rate p in pool 1. Proteins in any maturation state are transferred at a constant rate a from pool 1 to pool 2, but not in the opposite direction. Protein degradation occurs in both pools with different rate constants k_1 and k_2. The extended model, using one-step sfGFP maturation and two-step mCherry maturation can then be formulated as follows (indices 1 and 2 in N_x indicate pools 1 and 2):

$$dN_{d1,sfGFP} = pdt - \left(k_1 + m + a\right)N_{d1,sfGFP}dt \qquad \text{E42}$$

$$dN_{m1,sfGFP} = mN_{d1,sfGFP}dt - \left(k_1 \quad a\right)N_{m1,sfGFP}dt \qquad \text{E43}$$

$$dN_{d2,sfGFP} = aN_{d1,sfGFP}dt - \left(k_2 \quad m\right)N_{d2,sfGFP}dt \qquad \text{E44}$$

$$dN_{m2,sfGFP} = aN_{m1,sfGFP}dt + mN_{d2,sfGFP}dt - k_2 N_{m2,sfGFP}dt \qquad \text{E45}$$

$$dN_{d1,mCherry} = pdt - \left(k_1 + m_1 + a\right)N_{d1,mCherry}dt \qquad \text{E46}$$

$$dN_{i1,mCherry} = m_1 N_{d1,mCherry}dt - \left(k_1 + m_2 + a\right)N_{i1,mCherry}dt \qquad \text{E47}$$

$$dN_{m1,mCherry} = m_2 N_{i1,mCherry}dt - \left(k_1 \quad a\right)N_{m1,mCherry}dt \qquad \text{E48}$$

$$dN_{d2,mCherry} = aN_{d1,mCherry}dt - \left(k_2 \quad m_1\right)N_{d2,mCherry}dt \qquad \text{E49}$$

Nature Biotechnology: doi:10.1038/nbt.2281

$$dN_{i2,mCherry} = aN_{i1,mCherry}dt + m_1 N_{d2,mCherry}dt - \left(k_2 \quad m_2\right)N_{i2,mCherry}dt \qquad \text{E50}$$

$$dN_{m2,mCherry} = aN_{m1,mCherry}dt + m_2 N_{i2,mCherry}dt - k_2 N_{m2,mCherry}dt \qquad \text{E51}$$

Solving the two sets of differential equations (and considering FRET) provides the steady state mCherry/sfGFP intensity ratios in both pools:

$$\tilde{R}_1 = f\frac{\bar{N}_{m1,mCherry}}{\bar{N}_{m1,sfGFP}}\Bigg/\left(1-\frac{\bar{N}_{m1,mCherry}}{\bar{N}_{d1,mCherry}+\bar{N}_{i1,mCherry}+\bar{N}_{m1,mCherry}}E\right)$$
$$= \frac{m_1 m_2\left(a+k_1+m\right)}{m\left(a+k_1\right)\left(a+k_1+m_1\right)+mm_2\left(a+k_1+m_1\left(1-E\right)\right)} \qquad \text{E52}$$

$$\tilde{R}_2 = f\frac{\bar{N}_{m2,mCherry}}{\bar{N}_{m2,sfGFP}}\Bigg/\left(1-\frac{\bar{N}_{m2,mCherry}}{\bar{N}_{d2,mCherry}+\bar{N}_{i2,mCherry}+\bar{N}_{m2,mCherry}}E\right) \qquad \text{E53}$$

with the steady-state population sizes:

$$\bar{N}_{m2,sfGFP} = \frac{pam\left(a+k_1+k_2+m\right)}{k_2\left(a+k_1\right)\left(a+k_1+m\right)\left(k_2+m\right)} \qquad \text{E54}$$

$$\bar{N}_{d2,mCherry} = \frac{pa}{\left(a+k_1+m_1\right)\left(k_2+m_1\right)} \qquad \text{E55}$$

$$\bar{N}_{i2,mCherry} = \frac{pam_1\left(a+k_1+k_2+m_1+m_2\right)}{\left(a+k_1+m_1\right)\left(a+k_1+m_2\right)\left(k_2+m_1\right)\left(k_2+m_2\right)} \qquad \text{E56}$$

$$\bar{N}_{m2,mCherry} = \frac{pam_1m_2}{k_2\left(a+k_1\right)\left(a+k_1+m_1\right)\left(a+k_2+m_2\right)\left(k_2+m_1\right)\left(k_2+m_2\right)}$$
$$\cdot\left(a^2+k_1^2+\left(k_2+m_1\right)\left(k_2+m_2\right)+k_1\left(k_2+m_1+m_2\right)+a\left(2k_1+k_2+m_1+m_2\right)\right) \qquad \text{E57}$$

In this scenario, $\tilde{R}_2 > \tilde{R}_1$ in steady state. Using the kinetic parameters of the mCherry-sfGFP timer (m = log(2)/(5.63/60), m_1 = log(2)/(16.91/60), m_2 = log(2)/(30.30/60), E = 0.1733) and considering that $k_1 > 0$, $k_2 > 0$ and $a > 0$, the test for inequality $\tilde{R}_2 > \tilde{R}_1$ can be formulated as follows:

$$c_1\left(c_2+k_1\right)\left(c_3+k_1\right)\left(c_4+k_1\right)+\left(c_5+k_1\right)\left(c_6+k_1\right)\left(c_7+k_1\right)k_2+c_8k_2^2$$
$$+a^3\left(c_1+k_2\right)+a\left(c_9\left(c_{10}+k_1\right)\left(c_{11}+k_1\right)+3\left(c_{12}+k_1\right)\left(c_{13}+k_1\right)k_2\right) \qquad \text{E58}$$
$$+a^2\left(c_{14}+c_{15}k_2+k_1\left(c_9+3k_2\right)\right) \quad > 0$$

with constants:

Nature Biotechnology: doi:10.1038/nbt.2281

$$c_1 = 7.387, \quad c_2 = 1.37257, \quad c_3 = 2.45942, \quad c_4 = 3.4542, \quad c_5 = 1.64656,$$
$$c_6 = 2.25604, \quad c_7 = 7.31639, \quad c_8 = 0.585013, \quad c_9 = 22.161, \quad c_{10} = 1.82762, \qquad \text{E59}$$
$$c_{11} = 3.02984, \quad c_{12} = 1.94267, \quad c_{13} = 5.53666, \quad c_{14} = 53.8232, \quad c_{15} = 11.219$$

Since all constants are positive and $k_1 > 0$, $k_2 > 0$ and $a > 0$, this inequality is true and the intensity ratio in pool 2 (nuclear envelope) is always larger than in pool 1 (cytoplasm), independently of the effective degradation rate constants in the two pools (see Section 3.6).

Considering that NPCs are stable structures, scaffold nucleoporins should be transferred from the cytoplasm to the nuclear envelope (for assembly of new NPCs) but not in the opposite direction. The mCherry/sfGFP intensity ratio of such nucleoporins should be higher at the nuclear envelope than in the cytoplasm, as confirmed with fluorescence microscopy analysis of living cells (Fig. 3b, see also Supplementary Note 3).

Nature Biotechnology: doi:10.1038/nbt.2281

4 Supplementary Figures

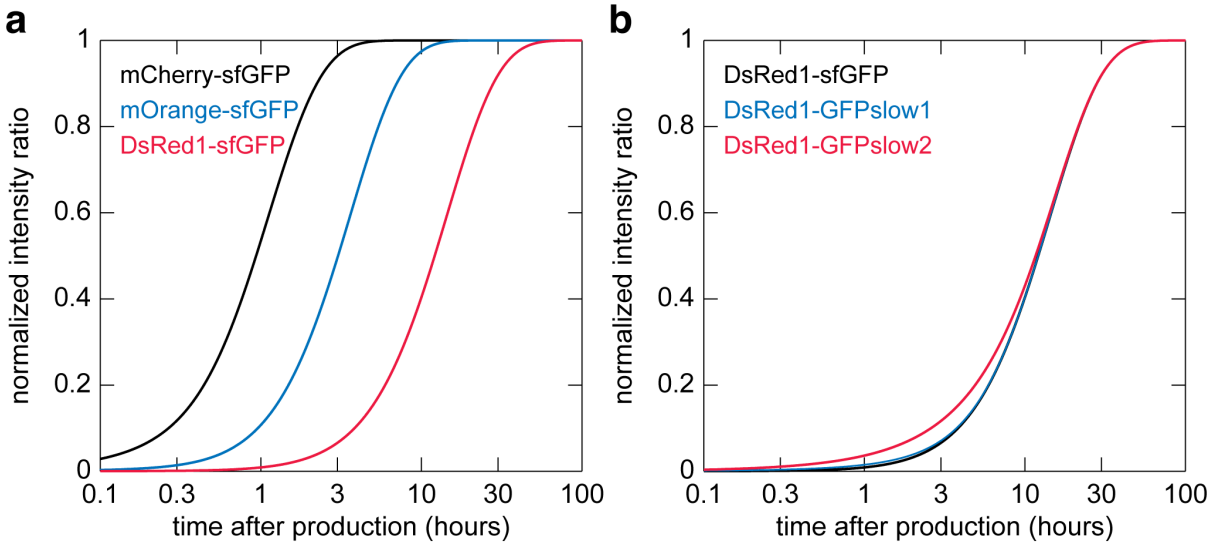

Supplementary Figure 1 | Time range of tFTs.
(**a**) tFTs composed of sfGFP (fast maturation) and red fluorescent proteins with different fluorophore maturation kinetics: mCherry (slow maturation) > mOrange > DsRed1 (very slow maturation). Ratios of fluorescence intensity of the red FPs divided by sfGFP fluorescence intensity are shown, normalized to the maximum in the plot. The curves with mOrange and DsRed1 were calculated using published maturation times[15] (see Section 3.7).
(**b**) tFTs composed of DsRed1 (very slow maturation) and green fluorescent proteins with different fluorophore maturation kinetics: sfGFP (fast maturation) > GFPslow1 > GFPslow2 (slow maturation). Ratios of fluorescence intensity of DsRed1 divided by fluorescence intensity of the green FPs are shown, normalized to the maximum in the plot. The curves with GFPslow1 and GFPslow2 were calculated using maturation half-times of 45 min (GFPslow1) and 2.5 h (GFPslow2) (see Section 3.7).

Nature Biotechnology: doi:10.1038/nbt.2281

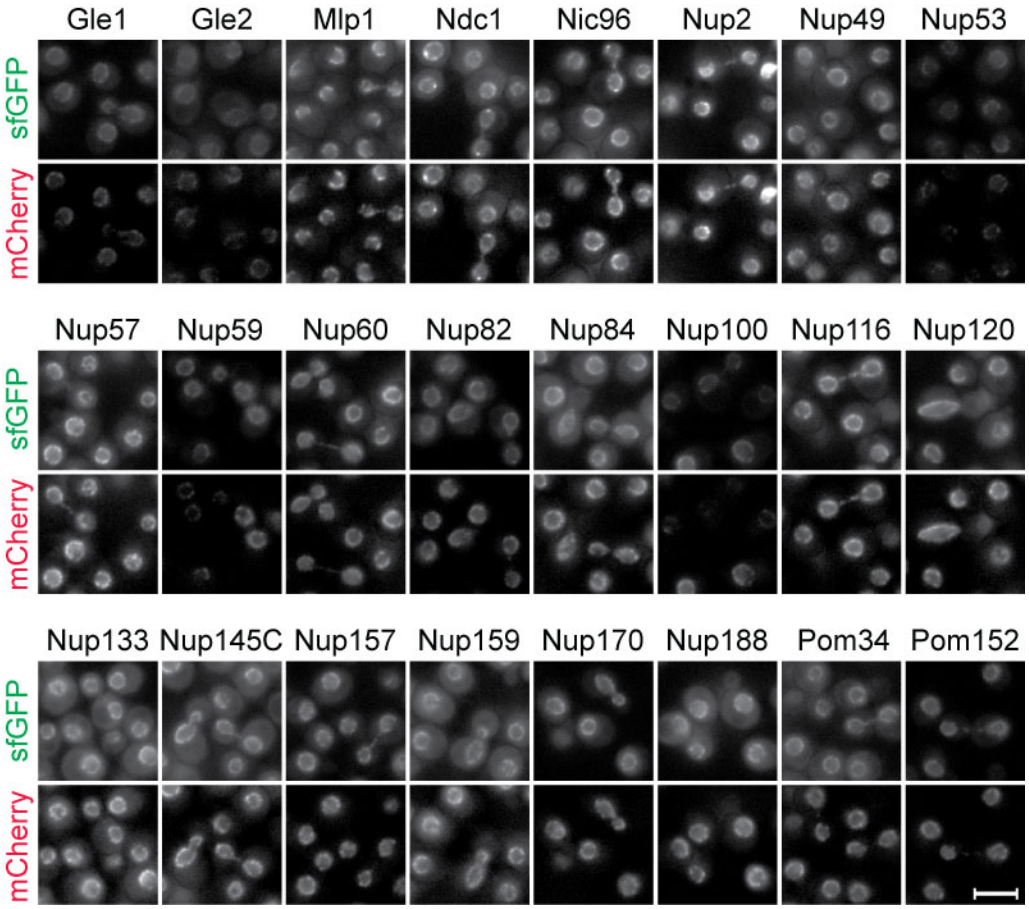

Supplementary Figure 2 | Fluorescence microscopy images of yeast cells with the indicated nucleoporins tagged chromosomally with mCherry-sfGFP and expressed from endogenous promoters. All images were acquired using the same exposure time and displayed using identical contrast settings. Scale bar: 5 µm. In total, 32 different nucleoporins were tagged with mCherry-sfGFP at the C-terminus. The following proteins were found to be non-functional when fused to mCherry-sfGFP: Mlp2, Nsp1, Nup1, Nup192, Nup42 and Nup85. The mCherry signal of the Seh1-mCherry-sfGFP fusion was not detectable by microscopy. Analysis of Sec13-mCherry-sfGFP was not possible because of its additional prominent localization to COPII vesicles[16,17].

Nature Biotechnology: doi:10.1038/nbt.2281

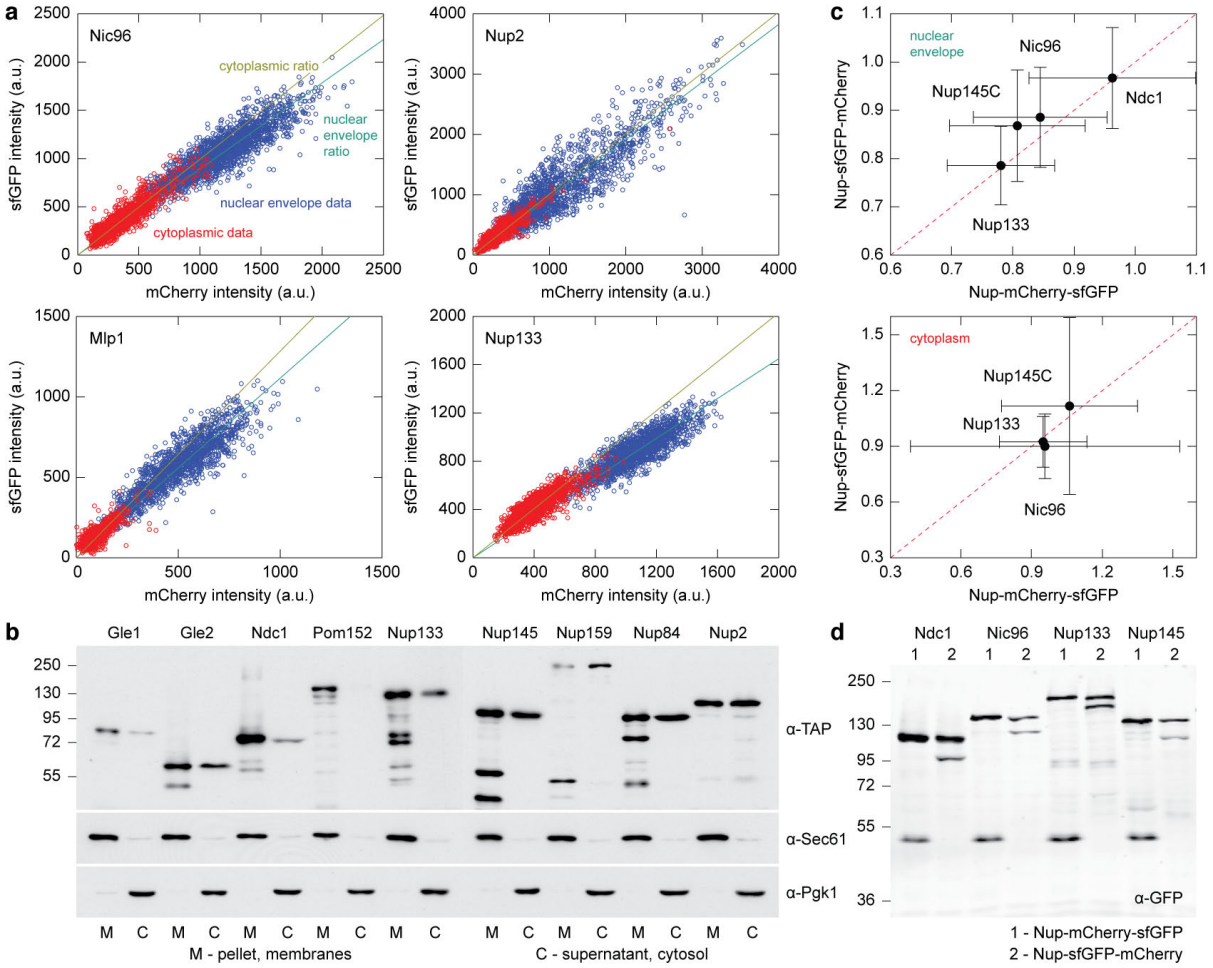

Supplementary Figure 3 | Identification of cytoplasmic nucleoporin pools and the effect of the order of fluorescent proteins in the mCherry-sfGFP timer.

(**a, b**) Significant cytoplasmic pools, within the sensitivity range of our imaging setup, were detected for most nucleoporins and confirmed by biochemical fractionation.

(**a**) Detection of cytoplasmic pools of nucleoporins fused to the mCherry-sfGFP timer. mCherry and sfGFP intensities of each nucleoporin were quantified at the nuclear envelope and in the cytoplasm using automated segmentation of fluorescence microscopy images (see Online Methods). Scatter plots of individual cell measurements are shown for the indicated nucleoporins (blue: nuclear envelope data; red: cytoplasmic data). Nuclear envelope and cytoplasmic data pools were subjected to linear regression. The resulting lines show the average intensity ratios at the nuclear envelope and in the cytoplasm. Note that the Nup2 measurement covers the entire dynamic range of the CCD chip (12 bit, grey levels measured between ~50 and ~3,700). A measurement bias is visible neither at the lower end nor at the upper end of the dynamic range.

(**b**) Biochemical fractionation revealed cytosolic pools for several nucleoporins. Strains expressing TAP-tagged nucleoporins from endogenous loci under the control of native promoters were grown at 30°C. Approximately 20 OD_{600} of cells were collected by centrifugation, re-suspended in LS-buffer (20 mM Hepes pH 7.6, 100 mM KOAc, 5 mM $Mg(OAc)_2$, 1 mM EDTA, 1 mM DTT, 0.1 mM PMSF and protease inhibitors (Complete™, Roche)) and lysed with glass beads by vortexing. Cell debris was removed by centrifugation at 1200 g for 2 min at 4°C. The cleared lysate was subjected to centrifugation at 6000 g for 20 min at 4°C. The resulting pellet (membranes) and supernatant (cytosol) were precipitated with trichloroacetic acid, resuspended in high-urea/SDS loading buffer[18], separated by SDS-PAGE followed by semi-dry blotting and probed with antibodies against the TAP tag (#Z0113, DAKO), Sec61[19] (kindly provided by Matthias Seedorf/ZMBH) and Pgk1 (#459250,

Nature Biotechnology: doi:10.1038/nbt.2281

Molecular Probes/Invitrogen). Control proteins for the membrane fraction (Sec61) and cytosol (Pgk1) were found in the pellet and supernatant, respectively. Transmembrane nucleoporins Ndc1 and Pom152 were found in the pellet fraction. In contrast, several components of the Nup84 complex (Nup133, Nup145C and Nup84), Nup159 and Nup2 exhibited substantial cytoplasmic fractions.
(**c, d**) The order of fluorescent proteins in the timer (sfGFP-mCherry instead of mCherry-sfGFP) did not affect the outcome of ratiometric analysis of nucleoporin fusions. This indicates that the local environment did not significantly influence the properties of the two FPs.
(**c**) The indicated nucleoporins were endogenously tagged with mCherry-sfGFP or sfGFP-mCherry at the C-terminus. sfGFP/mCherry intensity ratios (mean ± s.d., s.e.m. values are smaller than the black circles representing the data points) measured at the nuclear envelope and in the cytoplasm are shown for the two sets of strains.
(**d**) Whole cell extracts of all strains in (**c**) were separated by SDS-PAGE and probed with an antibody against GFP. The two fusion variants of each nucleoporin were expressed at similar levels. The apparent degradation products are the result of mCherry autohydrolysis during cell extract preparation[20].

Nature Biotechnology: doi:10.1038/nbt.2281

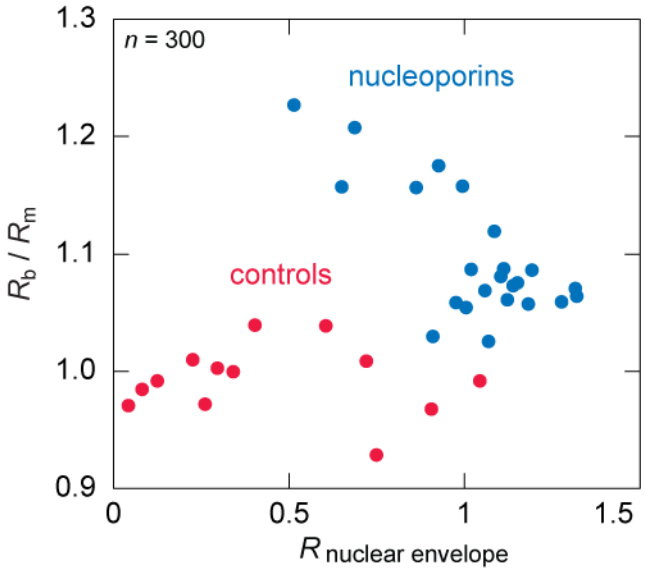

Supplementary Figure 4 | Correlation between the average mCherry/sfGFP intensity ratio at the nuclear envelope ($\boldsymbol{R}_{\text{nuclear envelope}}$) and the $\boldsymbol{R}_b/\boldsymbol{R}_m$ ratio measured for different nucleoporins tagged with mCherry-sfGFP (Fig. 3c). The $\boldsymbol{R}_b/\boldsymbol{R}_m$ ratios above 1 indicate that nucleoporins are on average older in the bud. However, the $\boldsymbol{R}_b/\boldsymbol{R}_m$ ratios also depend on the stability of the analyzed proteins because $\boldsymbol{R}$ does not scale linearly with protein degradation half-life (Supplementary Fig. 8b, c) and should approach 1 with increasing protein stability. This relationship is observed for nucleoporin using $\boldsymbol{R}_{\text{nuclear envelope}}$ as an approximate measure of stability, but not for control proteins (non-nucleoporins in Fig. 3c).

Nature Biotechnology: doi:10.1038/nbt.2281

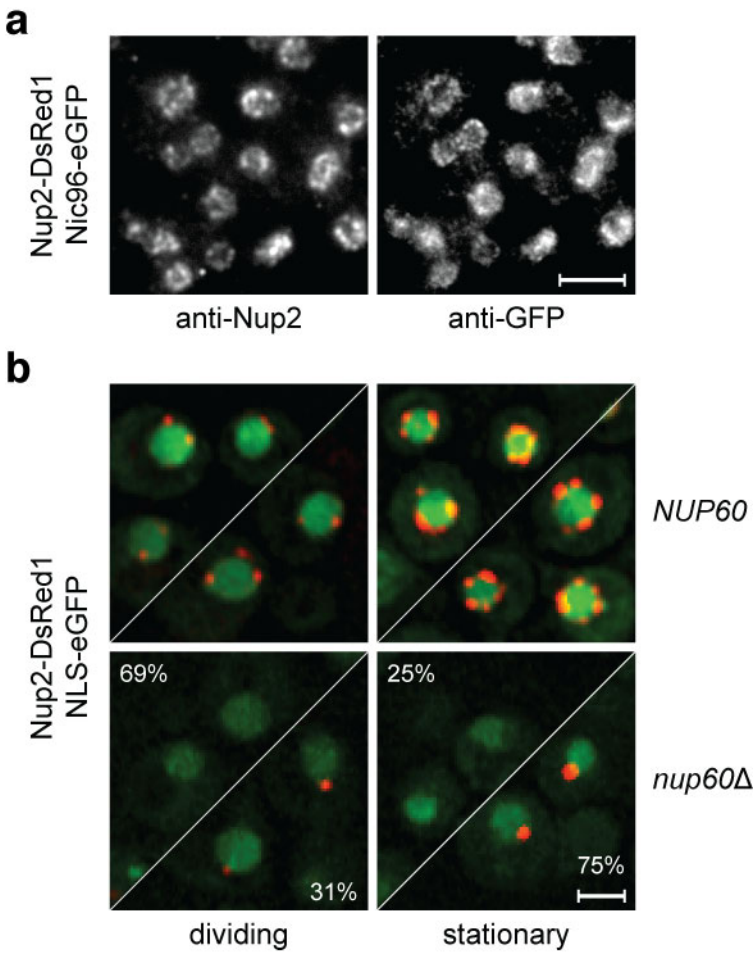

Supplementary Figure 5 | Validation of Nup2-DsRed1 localization to NPCs.
(**a**) Cells expressing the Nup2-DsRed1 and Nic96-eGFP fusions were processed for detection of Nup2 (using Mab414) and GFP (using anti-GFP antibodies) by immunofluorescence. Mab414 is specific for XFXFG nucleoporins and recognizes predominantly Nup2, but also weakly Nsp1[21], as verified with a *nup2*Δ control strain (data not shown). Scale bar: 5 µm.
(**b**) Nup2-DsRed1 marks old NPCs. Fluorescence microscopy of live wild type (*NUP60*) and *nup60*Δ cells expressing Nup2-DsRed1 and the nuclear marker NLS-eGFP. Wild type dividing cells carried only a few red dots per nucleus. Their number and intensity increased when cells stopped growing (stationary, 2-3 days of starvation), which allowed DsRed1 to mature. Nup2-DsRed1 was anchored to the nuclear periphery via the NPC component Nup60, as expected[22]. The single Nup2-DsRed1 dot observed in some *nup60*Δ cells is probably the results of Nup2-DsRed1 oligomerization due to the tetrametic nature of DsRed1. Maximum projections of z-stacks are shown. Scale bar: 2 µm.

Nature Biotechnology: doi:10.1038/nbt.2281

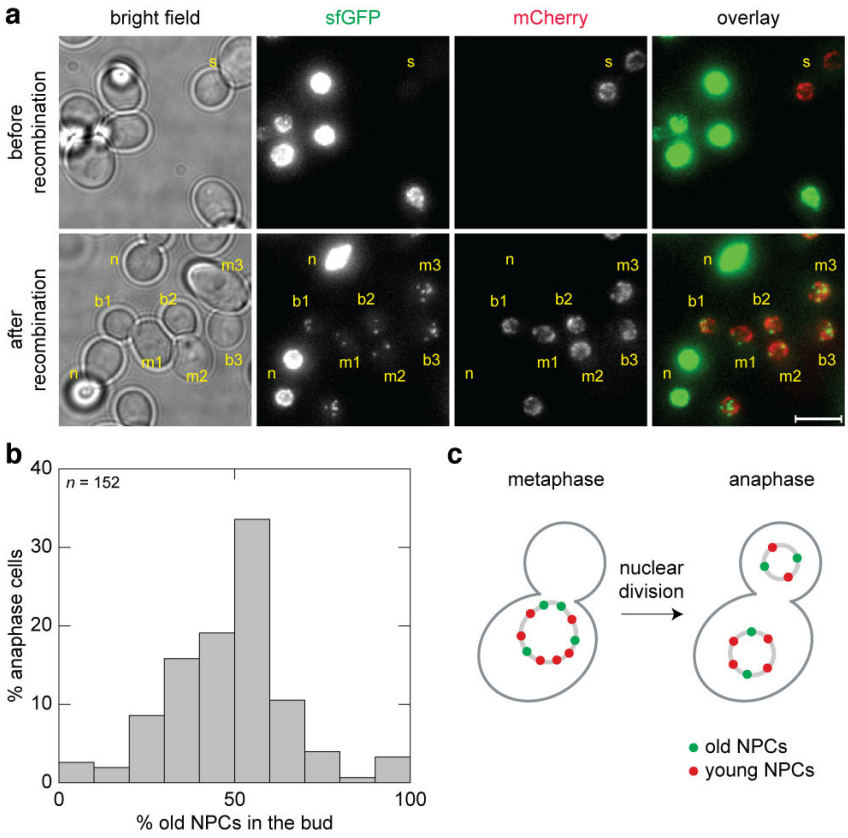

Supplementary Figure 6 | Analysis of segregation of old NPCs with recombination-induced tag exchange (RITE). RITE permits the regulated exchange of one tag with a second one at the level of DNA using Cre recombinase-mediated excision of the first tag sequence. RITE therefore allows differential labeling of old and new protein molecules in a time-controlled manner[23]. We applied RITE to Nic96, a stable component of the nuclear pore complex.

(**a**) *NIC96* was chromosomally tagged with the RITE cassette (*loxP-sfGFP-STOP-loxP-mCherry*) in a strain carrying a conditional Cre recombinase. Such cells expressed Nic96-sfGFP before activation of Cre recombinase and spontaneous recombination (s) occurred at low frequency. After activation of Cre recombinase by addition of β-estradiol to the growth medium[23] and recombination between the *loxP* sites, Nic96-mCherry was expressed instead of Nic96-sfGFP. Only some cells failed to undergo recombination (n). As Nic96 is stably incorporated into NPCs, Nic96-sfGFP remained at pre-existing NPCs for several generations after recombination. The number of NPCs labeled with Nic96-sfGFP (old NPCs) was counted in pairs of mother (m) and bud (b) cells that underwent recombination. Shown are representative fields of view before and after induction of recombination (maximum projections of z-stacks). Scale bar: 5 µm.

(**b**) Distribution of old NPCs (labeled with Nic96-GFP) after recombination-induced tag exchange in cells from (**a**) that contained in total less than 20 single green NPCs. On average 47 ± 18 % of old NPCs (mean ± s.d., n = 152 mother/bud pairs) were segregated into the bud. As the bud receives ~38% of all NPCs and nuclear envelope[5,24], this result indicates that the density of old NPCs is 1.45 ± 0.55 (mean ± s.d.) times higher in the bud than in the mother, in remarkable agreement with the Nup2-DsRed1 analysis (see main text).

(**c**) Cartoon of age-dependent distribution of NPCs in yeast mitosis. *S. cerevisiae* undergoes closed mitosis, whereby the nuclear envelope stays intact and NPCs do not disassemble. NPCs are partitioned during nuclear division such that mother and bud nuclei receive approximately the same absolute number of old NPCs. In relative terms, the density of old NPCs in the bud is ~1.5 times higher than in the mother.

Nature Biotechnology: doi:10.1038/nbt.2281

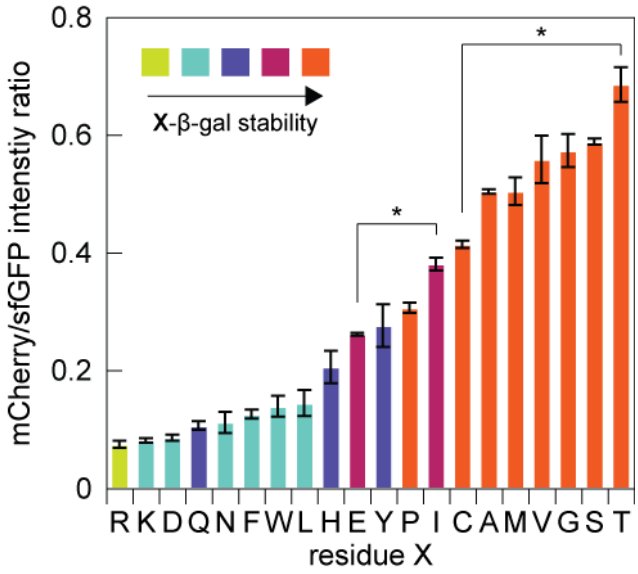

Supplementary Figure 7 | Ratiometric flow cytometry analysis of cells expressing Ubi-**X**-mCherry-sfGFP constructs with the indicated residues at position **X**. Ubi-**X**-mCherry-sfGFP constructs are colored according to the half-lives of corresponding **X**-β-galactosidase fusions, determined using pulse-chase experiments with metabolic labeling[25,25,26]. Measurement of the degradation kinetics of **X**-β-gal fusions led to the definition of the N-end rule, that grouped the twenty standard amino acids into five stability groups[25,26]. Our fluorescence measurements with flow cytometry recapitulated the pulse-chase results and revealed additional differences in stability conferred by amino acids within the same stability group. For example, N-terminal glutamic acid (E) was more destabilizing than isoleucine (I), or threonine (T) was more stabilizing than cysteine (C) (*, $p < 0.01$). Error bars indicate s.d. ($n = 3$). Of note, the tFT reports on the average turnover of all intermediate species formed from Ubi-**X**-mCherry-sfGFP. Thus, although proline (P) is a highly stabilizing residue, removal of N-terminal ubiquitin from Ubi-P-β-gal is inefficient and full length Ubi-P-β-gal is rapidly degraded by the UFD (ubiquitin-fusion degradation) pathway[26,27]. The combination of these effects explains the intermediate mCherry/sfGFP intensity ratio, indicative of significant turnover, of cells expressing Ubi-P-mCherry-sfGFP.

Nature Biotechnology: doi:10.1038/nbt.2281

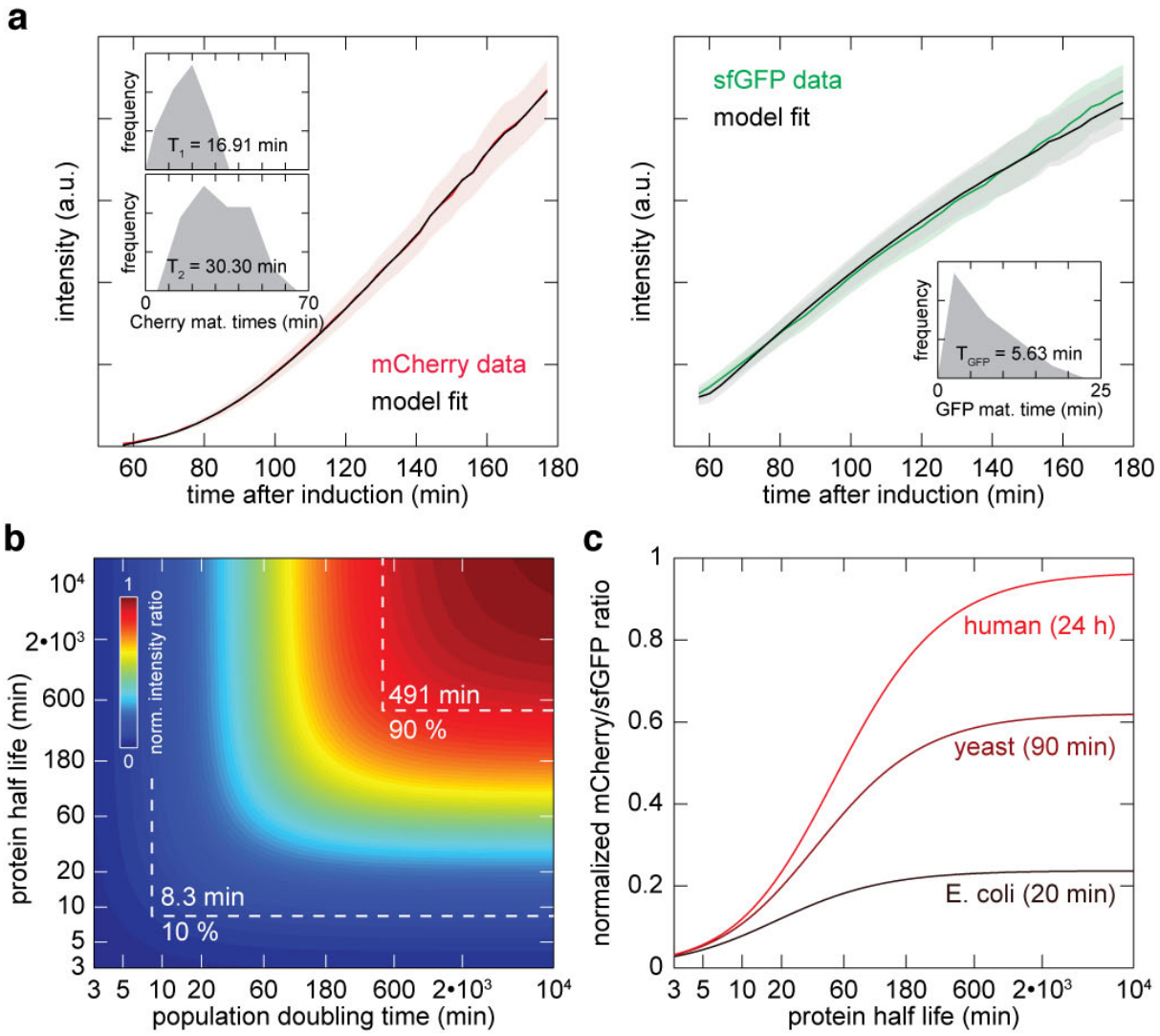

Supplementary Figure 8 | Characterization of the mCherry-sfGFP timer.
(**a**) Cells induced to express a non-degradable mCherry-sfGFP fusion (strain AK1212 carrying the Ubi-M-RR-mCherry-sfGFP construct, which contains two lysine-to-arginine mutations in the degron sequence) were imaged with a fluorescence microscope. Maturation rate constants of mCherry and sfGFP were determined by fitting theoretical maturation models to fluorescence intensity traces of single cells (see Section 1.2). A two-step maturation model for mCherry fitted the data (maturation half-times: $T_{mCherry,1}$ = 16.9 ± 7.3 min, $T_{mCherry,2}$ = 30.3 ± 11.2 min, mean ± s.d., n = 35). Note that m (maturation rate constant) = ln(2) / T. No reasonable fit could be achieved using a single-step maturation model. The average induction curves and model fits are shown with one standard deviation. The time after start of induction is indicated. Insets show the distributions of maturation half-times obtained from single-cell fitting.
(**b**) Dynamic range of the mCherry-sfGFP timer. mCherry/sfGFP intensity ratios were calculated as a function of protein stability and population doubling time (see Section 3.6) using the experimentally determined maturation parameters of the two FPs and the FRET efficiency of the timer. The area delimited by dashed white lines indicates the domain of half-lives/doubling times that can be resolved using the central 80% of the total dynamic range provided by the mCherry-sfGFP timer.
(**c**) The dynamic range of mCherry-sfGFP is plotted for three typical population doubling times.

Nature Biotechnology: doi:10.1038/nbt.2281

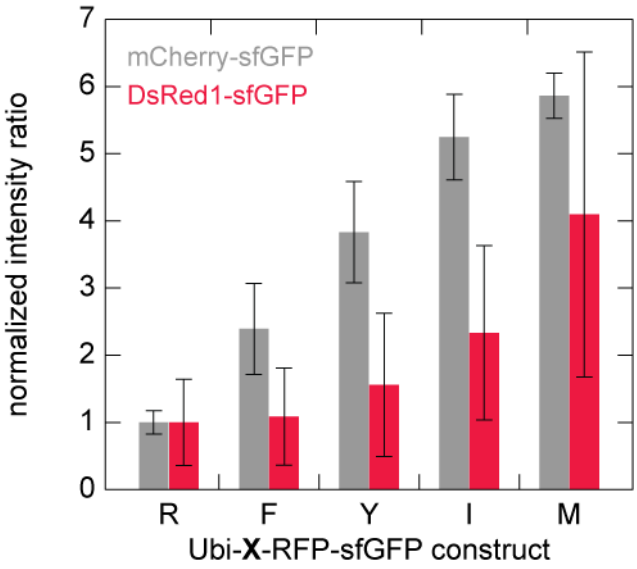

Supplementary Figure 9 | Comparison of mCherry-sfGFP and DsRed1-sfGFP timers composed of different red fluorescent proteins (RFPs) fused to sfGFP. Cells expressing Ubi-**X**-RFP-sfGFP constructs of different stabilities (**X** = R (unstable) < F < Y < I < M (stable)) were analyzed using fluorescence microscopy. RFP/sfGFP intensity ratios are shown (median ± m.a.d., $n > 40$ cells), normalized to the most unstable construct. Consistent with the idea that the slow maturing fluorescent protein determines the time range of a tFT, only the most stable constructs could be distinguished with the DsRed1-sfGFP timer. Aggregation of Ubi-**X**-DsRed1-sfGFP fusion proteins and low fluorescence intensity levels in the DsRed1 channel contribute to the observed large cell-to-cell variability.

Nature Biotechnology: doi:10.1038/nbt.2281

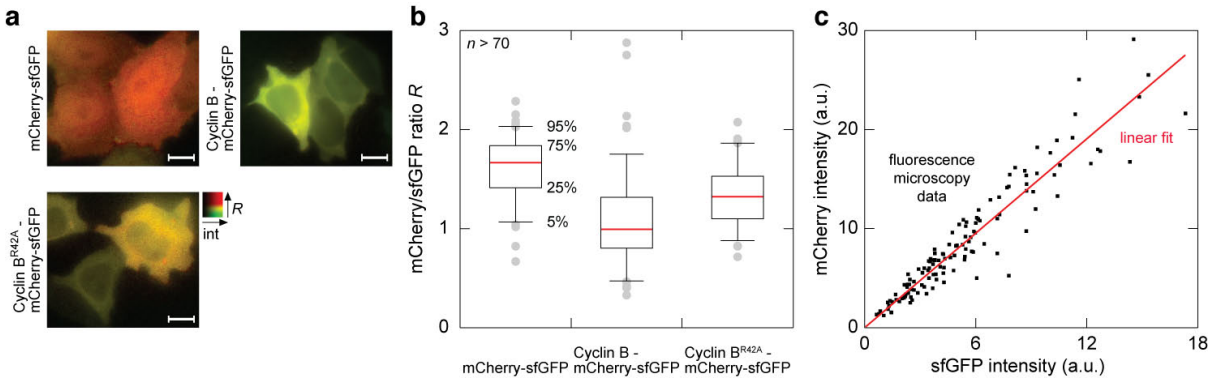

Supplementary Figure 10 | Snapshot analysis of protein stability in mammalian cells. mCherry-sfGFP was expressed in HeLa cells either alone, fused to the unstable protein cyclin B or fused to a stabilized mutant of cyclin B with an impaired destruction box (cyclin B^{R42A})[28].

(**a**) Intensity-weighted ratiometric images of cells expressing the indicated constructs. Scale bars: 10 µm.

(**b**) Ratiometric analysis of cells from (**a**). Median values are marked with red bars. All differences are statistically significant ($p < 10^{-4}$ in an unpaired *t*-test, n > 70 cells for each construct). Thus, the mCherry/sfGFP intensity ratio faithfully reports on the average degradation kinetics of different constructs in HeLa cells.

(**c**) sfGFP and mCherry intensities of single cells expressing mCherry-sfGFP. The mCherry/sfGFP intensity ratio is independent of the expression levels, in agreement with the theoretical description of mCherry-sfGFP turnover (Supplementary Note 4).

Nature Biotechnology: doi:10.1038/nbt.2281

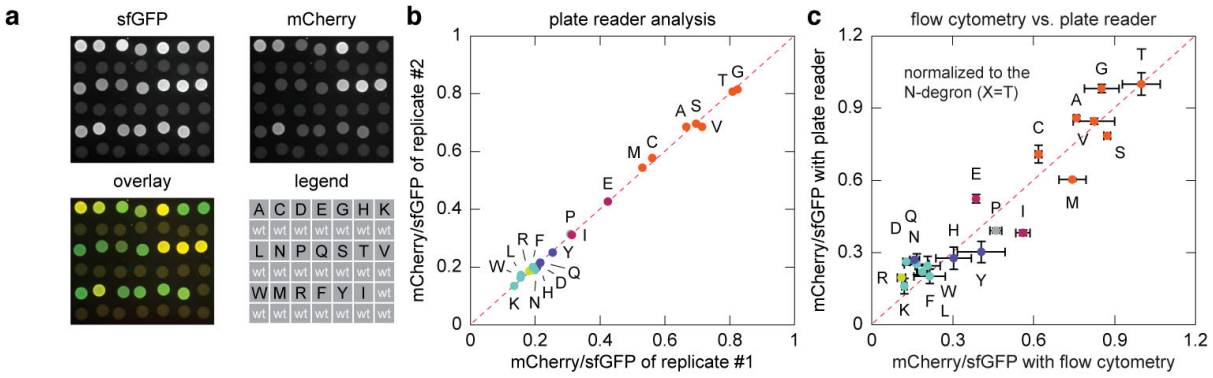

Supplementary Figure 11 | Whole colony imaging with a fluorescence plate reader.
(**a**) Shown are images of an agar plate with colonies of strains expressing different Ubi-**X**-mCherry-sfGFP fusions, with the corresponding residues at position **X** indicated in the legend panel.
(**b**) Reproducibility of fluorescence plate reader measurements. mCherry/sfGFP intensity ratios of the indicated strains in two independent replicates of the plate shown in (**a**). The strains are color-coded according to Supplementary Figure 7. All measurements were corrected for colony autofluorescence using fluorescence measurements of a wild type strain (wt) that did not express any fluorescent proteins.
(**c**) Comparison of fluorescence intensity ratios measured with flow cytometry and plate reader. Fluorescence intensities of single cells growing in liquid medium were measured with flow cytometry and combined into an mCherry/sfGFP intensity ratio of the population. Fluorescence intensities of whole colonies growing on solid medium were measured with a fluorescence plate reader. Despite these differences, the mCherry/sfGFP intensity ratios of strains expressing the indicated Ubi-**X**-mCherry-sfGFP fusions determined with the two techniques are in remarkable agreement. The strains are color-coded according to Supplementary Figure 7. Error bars indicate s.d. ($n = 2$ replicates for plate reader measurements, $n = 3$ replicates for flow cytometry measurements). We note that fluorescence plate reader measurements are less sensitive and fusions expressed at low levels are difficult to detect with whole colony measurements. Strains expressing the most unstable, and thus less abundant, Ubi-**X**-mCherry-sfGFP fusions are reliably distinguished from each other with flow cytometry but not plate reader measurements. However, plate reader measurements have the advantage of allowing simultaneous measurement of multiple samples (up to 1536 colonies) on one plate.

Nature Biotechnology: doi:10.1038/nbt.2281

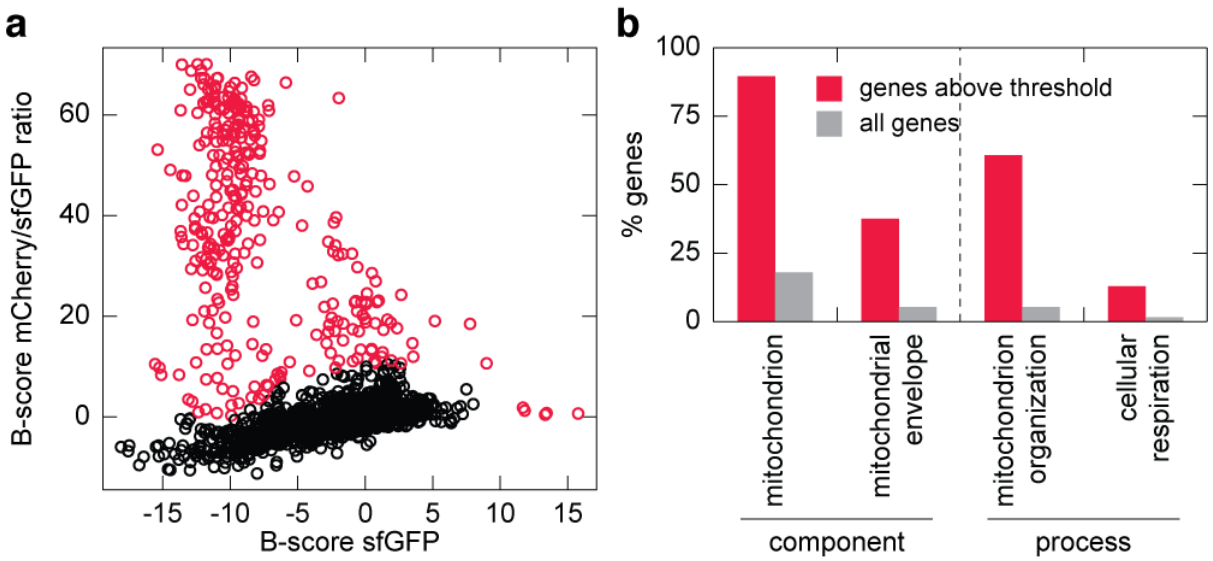

Supplementary Figure 12 | Identification of false-positive hits in the control screen with the non-degradable mCherry-sfGFP fusion.
(**a**) Behavior of the non-degradable control fusion (Fig. 5b) in a genome-wide library of yeast gene deletion strains. The sfGFP fluorescence intensity and the mCherry/sfGFP intensity ratio of each strain in one screen replicate are represented by normalized B-scores (see Online Methods). ~250 strains that strongly affected the non-degradable control (colored in red) were identified in an automated fashion and omitted from further analysis.
(**b**) The set of strains colored in red in (a) was mapped to "component" and "function" sets of Yeast-GO Slim terms, and compared to all protein-coding genes of *S. cerevisiae* (all genes). This analysis showed that the behavior of the non-degradable control fusion is affected mostly by deletions of mitochondrial components or factors involved in mitochondrial function.

Nature Biotechnology: doi:10.1038/nbt.2281

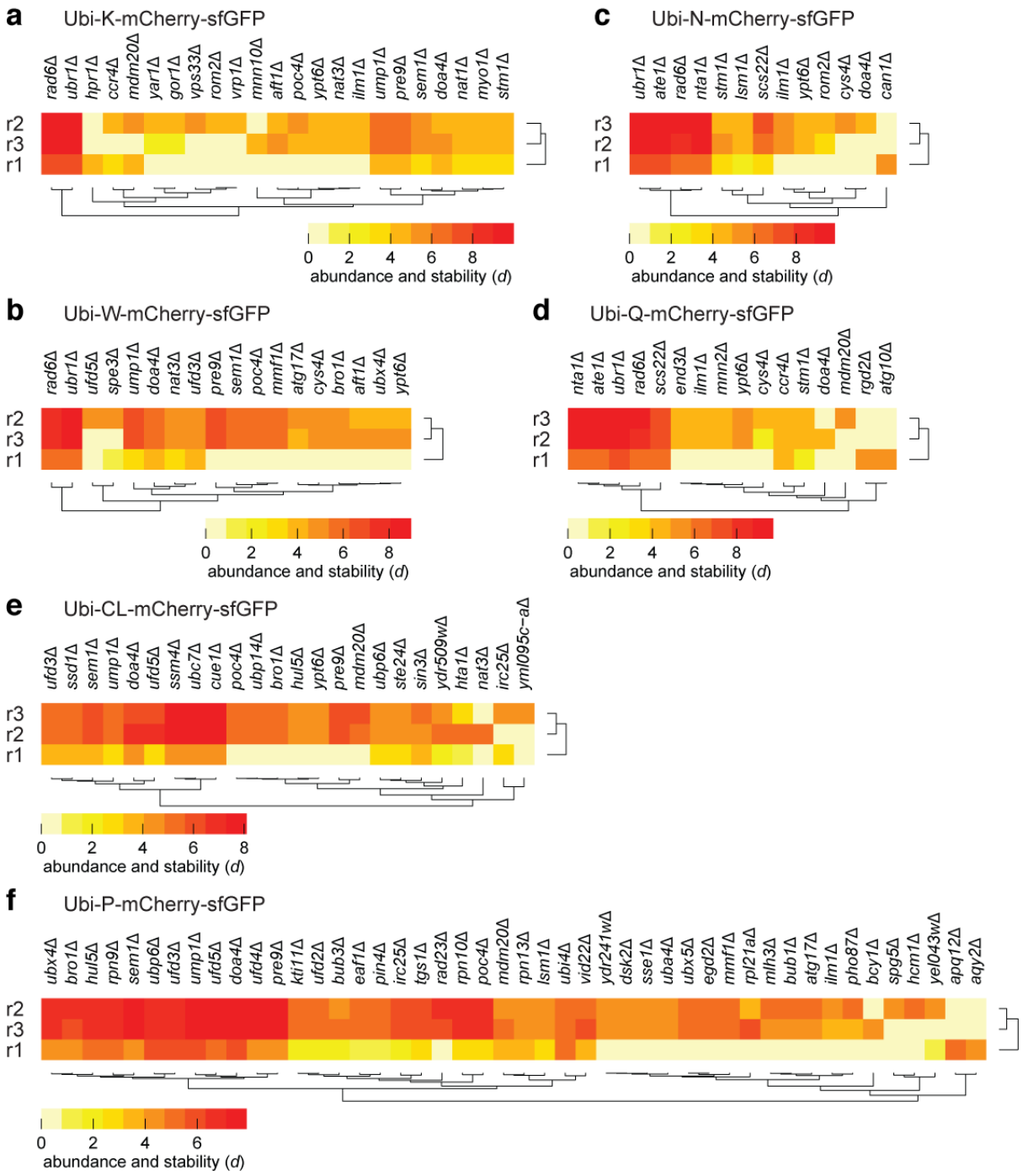

Supplementary Figure 13 | Comparison between replicate screens.
Three replicate screens (r1, r2, r3) were performed with each Ubi-X(Z)-mCherry-sfGFP construct (Fig. 5b). For replicates r2 and r3, strains with deletions of essentials genes were removed from the genome-wide library of heterozygous diploid knockout strains, and the library was condensed to eliminate empty plate positions. This is expected to decrease variability in colony fluorescence caused by differences in colony size as colonies with neighboring empty positions have access to more nutrients and grow at increased rate. Replicates r2 and r3 were imaged on the Decon imaging station (see Online Methods) with a more uniform illumination of increased power compared to the Kodak fluorescence imager used for replicate r1. (**a-f**) Deletion strains with $d > 4.5$ (see Online Methods) in at least one replicate were included in the heat maps.

Nature Biotechnology: doi:10.1038/nbt.2281

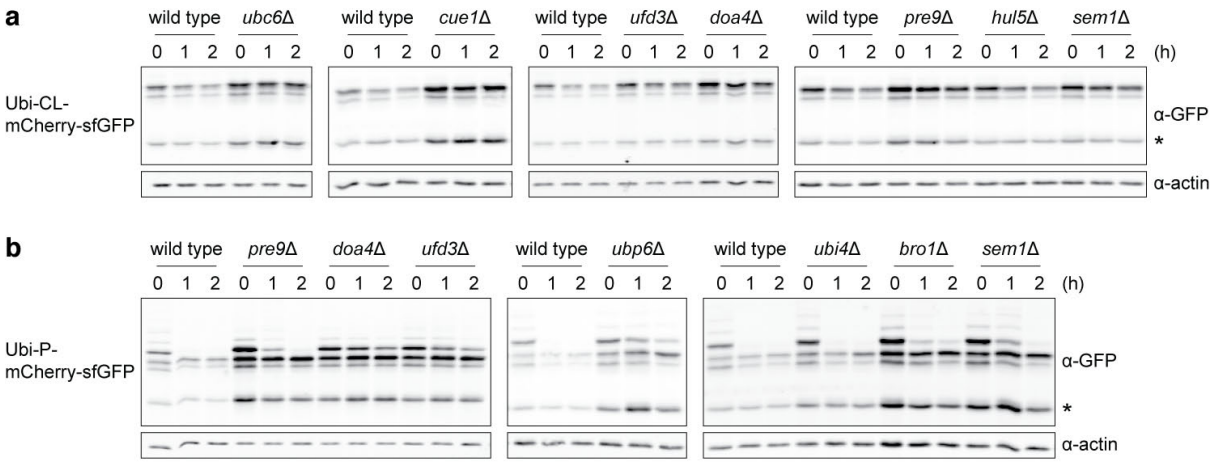

Supplementary Figure 14 | Validation of Ubi-CL-mCherry-sfGFP and Ubi-P-mCherry-sfGFP stabilization in strains lacking different components of the ubiquitin-proteasome system.
(**a**) Cycloheximide chase experiments with the indicated strains expressing Ubi-CL-mCherry-sfGFP. Strains were grown to OD_{600} 0.6-1.0 in SC-glucose medium at 30°C and cycloheximide (C7698, Sigma, Germany) was added to final concentration of 0.1 mg/ml. Samples were collected at the indicated time points by centrifugation at 3000 g for 5 min and flash frozen in liquid nitrogen. Whole cell extracts were prepared as previously described[18], separated by SDS-PAGE followed by semi-dry blotting and probed with rabbit anti-GFP and mouse anti-actin (mAB1501, Chemicon/Millipore) antibodies. Secondary antibodies labeled with $Alexa_{680}$ (Invitrogen, Germany) or $IRDye_{800}$ (Rockland Immunochemicals Inc., USA) were used for detection with an Odyssey Infrared Imaging System (LI-Cor Biosystems, Germany). Membranes were scanned at 700 and 800 nm wavelengths with a resolution of 169 µm in medium quality. A product of mCherry autohydrolysis during cell extract preparation[20] is marked with an asterisk (*). Ubi-CL-mCherry-sfGFP is visibly stabilized by deletion of *CUE1, UBC6, UFD3, DOA4, PRE9* and *SEM1*, consistent with the results from the screens (Fig. 5f).
(**b**) Cycloheximide chase experiments with the indicated strains expressing Ubi-P-mCherry-sfGFP analyzed as in (**a**). Ubi-P-mCherry-sfGFP is stabilized by deletion of *PRE9, DOA4, UFD3, UBP6, UBI4, BRO1 and SEM1*.

Nature Biotechnology: doi:10.1038/nbt.2281

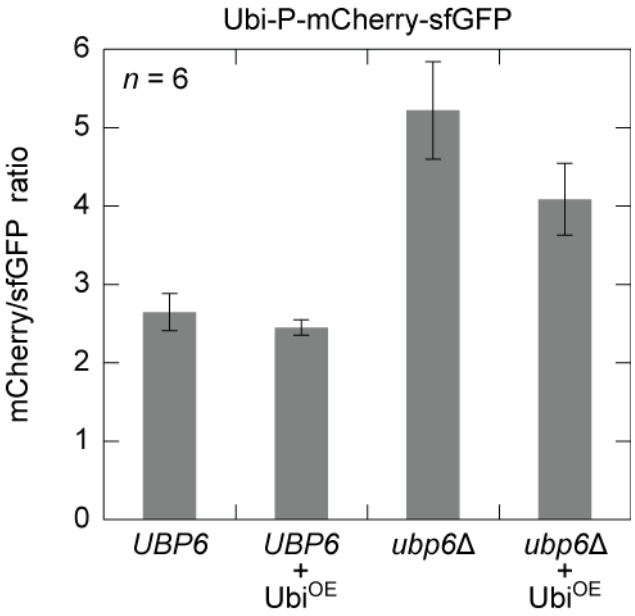

Supplementary Figure 15 | Ubiquitin overexpression partially suppresses the stabilization of Ubi-P-mCherry-sfGFP in the *ubp6*Δ mutant. Quantification of whole colony mCherry/sfGFP intensity ratios of wild type (*UBP6*) and *ubp6*Δ strains transformed with a control plasmid (YEp195) or a high copy number plasmid for ubiquitin overexpression under the control of the *CUP1* promoter (Ubi^{OE}). Error bars indicate s.d. (n = 6 replicates for each genotype). The mCherry/sfGFP intensity ratios of *ubp6*Δ strains with and without Ubi^{OE} differ significantly ($p < 0.005$).

Nature Biotechnology: doi:10.1038/nbt.2281

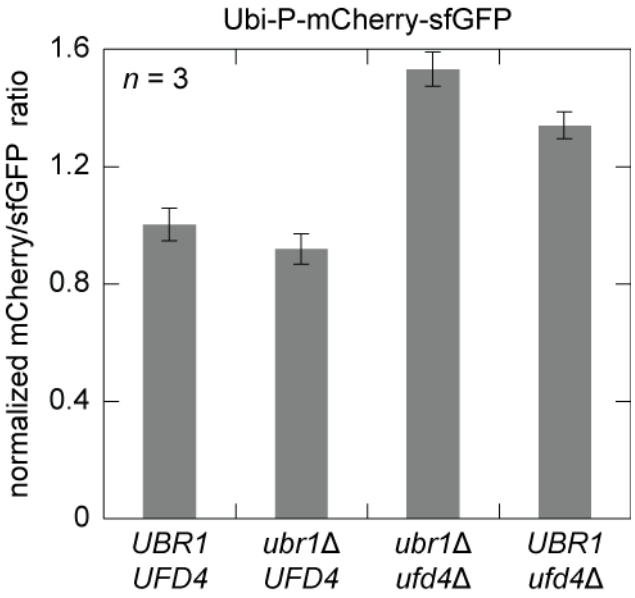

Supplementary Figure 16 | Ubr1 and Ufd4 cooperate in degradation of ubiquitin-fusions *in vivo*. Quantification of whole colony mCherry/sfGFP intensity ratios, normalized to the wild type *UBR1 UFD4* strain. Error bars indicate s.d. (n = 3 replicates for each genotype). The mCherry/sfGFP intensity ratios of *ubr1*Δ *ufd4*Δ and *UBR1 ufd4*Δ strains differ significantly ($p < 0.012$). The increased stabilization of Ubi-P-mCherry-sfGFP by deletion of *UBR1* in *ufd4*Δ background could not be detected by pulse-chase with radiolabeling and inhibition of protein synthesis[29]. This is probably explained by the significant experimental error associated with sample processing for pulse-chase analysis, which precludes distinguishing protein with similar stabilities (see also Supplementary Fig. 7). Analysis of protein stability with tFTs is performed directly in living cells, without any sample processing, justifying the sensitivity of this approach.

Nature Biotechnology: doi:10.1038/nbt.2281

5 Supplementary Tables

5.1 Supplementary Table 1

Yeast strains used in this study.

Name	Background	Description	used in Figure/Reference
FY1679	S288c	MATa/α ura3-52/ura3-52 trp1Δ63/TRP1 leu2Δ1/LEU2 his3Δ200/HIS3 GAL2+/GAL2+	EUROFAN reference strain
ESM356-1	FY1679	MATa ura3-52 leu2Δ1 his3Δ200 trp1Δ63	Spore of FY1679
ESM356-2	FY1679	MATa ura3-52 leu2Δ1 trp1Δ63	Spore of FY1679
ESM357-1	FY1679	MATα ura3-52 leu2Δ1 his3Δ200	Spore of FY1679
AK1027	ESM356-1	SPC42-mCherry-sfGFP-kanMX	2
AK1216	AK1027	SPC42-mCherry-sfGFP-kanMX kar9Δ::hphNT1	2
AK1092	ESM356-1	HXT1-mCherry-sfGFP-kanMX	2
AK1093	ESM356-1	PMA1-mCherry-sfGFP-kanMX	2
AK1110	ESM356-2	RAX2-mCherry-sfGFP-kanMX	
AK1111	ESM357-1	RAX2-mCherry-sfGFP-kanMX	
AK1112	AK1110xAK1111	RAX2-mCherry-sfGFP-kanMX/RAX2-mCherry-sfGFP-kanMX	2
AK728	ESM356-1	GLE1-mCherry-sfGFP-kanMX	3, S2, S4
AK729	ESM356-1	GLE2-mCherry-sfGFP-kanMX	3, S2, S4
AK730	ESM356-1	MLP1-mCherry-sfGFP-kanMX	3, S2, S3, S4
AK732	ESM356-1	NDC1-mCherry-sfGFP-kanMX	3, S2, S3, S4
AK733	ESM356-1	NIC96-mCherry-sfGFP-kanMX	3, S2, S3, S4
AK744	ESM356-1	NUP2-mCherry-sfGFP-kanMX	3, S2, S3, S4
AK745	ESM356-1	NUP49-mCherry-sfGFP-kanMX	3, S2, S4
AK746	ESM356-1	NUP53-mCherry-sfGFP-kanMX	3, S2
AK747	ESM356-1	NUP57-mCherry-sfGFP-kanMX	3, S2, S4
AK748	ESM356-1	NUP59-mCherry-sfGFP-kanMX	3, S2, S4
AK749	ESM356-1	NUP60-mCherry-sfGFP-kanMX	3, S2, S4
AK750	ESM356-1	NUP82-mCherry-sfGFP-kanMX	3, S2, S4
AK751	ESM356-1	NUP84-mCherry-sfGFP-kanMX	3, S2, S4
AK736	ESM356-1	NUP100-mCherry-sfGFP-kanMX	3, S2, S4
AK971	ESM356-1	NUP116-mCherry-sfGFP-kanMX	3, S2, S4
AK972	ESM356-1	NUP120-mCherry-sfGFP-kanMX	3, S2, S4
AK737	ESM356-1	NUP133-mCherry-sfGFP-kanMX	3, S2, S3, S4
AK738	ESM356-1	NUP145-mCherry-sfGFP-kanMX	3, S2, S3, S4
AK739	ESM356-1	NUP157-mCherry-sfGFP-kanMX	3, S2, S4
AK740	ESM356-1	NUP159-mCherry-sfGFP-kanMX	3, S2, S4
AK741	ESM356-1	NUP170-mCherry-sfGFP-kanMX	3, S2, S4
AK742	ESM356-1	NUP188-mCherry-sfGFP-kanMX	3, S2, S4
AK754	ESM356-1	POM34-mCherry-sfGFP-kanMX	3, S2, S4
AK753	ESM356-1	POM152-mCherry-sfGFP-kanMX	3, S2, S4

Nature Biotechnology: doi:10.1038/nbt.2281

Name	Background	Description	used in Figure/Reference
AK645	ESM356-1	CDC14-mCherry-sfGFP-kanMX	3, S4
yMaM171	ESM356-1	NSG1-mCherry-sfGFP-kanMX	3, S4
yMaM172	ESM356-1	SEC61-mCherry-sfGFP-kanMX	3, S4
yMaM178	ESM356-1	natNT2-TEF-mCherry-sfGFP-PRM3	3, S4
AK1105	ESM356-1	YPR174C-mCherry-sfGFP-kanMX	3, S4
AK1108	ESM356-1	HMG1-mCherry-sfGFP-kanMX	3, S4
AK1109	ESM356-1	HMG2-mCherry-sfGFP-kanMX	3, S4
AK1107	ESM356-1	HEH2-mCherry-sfGFP-kanMX	3, S4
AK1098	ESM356-1	NUP2-DsRed1-kanMX ura3::NLS-eGFP::URA3	3, S5
yMaM82	ESM356-1	ura3::kanMX-GDP^{pr}-Ubi-M-mCherry-sfGFP::ura3	4, S7, S11
yMaM83	ESM356-1	ura3::kanMX-GDP^{pr}-Ubi-I-mCherry-sfGFP::ura3	4, S7, S11
yMaM84	ESM356-1	ura3::kanMX-GDP^{pr}-Ubi-F-mCherry-sfGFP::ura3	4, S7, S11
yMaM85	ESM356-1	ura3::kanMX-GDP^{pr}-Ubi-M-mCherry-sfGFP::ura3 ubr1Δ::hphNT1	4
yMaM86	ESM356-1	ura3::kanMX-GDP^{pr}-Ubi-I-mCherry-sfGFP::ura3 ubr1Δ::hphNT1	4
yMaM87	ESM356-1	ura3::kanMX-GDP^{pr}-Ubi-F-mCherry-sfGFP::ura3 ubr1Δ::hphNT1	4
yMaM94	ESM356-1	ura3::kanMX-GDP^{pr}-Ubi-M-mCherry-sfGFP::ura3 natNT2-GDP^{pr}::UBR1	4
yMaM95	ESM356-1	ura3::kanMX-GDP^{pr}-Ubi-I-mCherry-sfGFP::ura3 natNT2-GDP^{pr}::UBR1	4
yMaM96	ESM356-1	ura3::kanMX-GDP^{pr}-Ubi-F-mCherry-sfGFP::ura3 natNT2-GDP^{pr}::UBR1	4
yMaM38	ESM356-1	p415-GDP^{pr}-Ubi-M-mCherry-sfGFP	4, S9
yMaM108	ESM356-1	p415-GDP^{pr}-Ubi-Y-mCherry-sfGFP	4, S9
yMaM57	ESM356-1	p415-TEF^{pr}-Ubi-M-mCherry-sfGFP	4
yMaM58	ESM356-1	p415-TEF^{pr}-Ubi-Y-mCherry-sfGFP	4
yMaM59	ESM356-1	p415-GAL1^{pr}-Ubi-M-mCherry-sfGFP	4
yMaM63	ESM356-1	p415-GAL1^{pr}-Ubi-Y-mCherry-sfGFP	4
Y8205	–	MATα his3Δ1 leu2Δ0 ura3Δ0 met15Δ0 can1Δ::STE2^{pr}-his5 lyp1Δ::STE3^{pr}-LEU2	Ref[30]
YAnB61	Y8205	ura3::natMX-GDP^{pr}-Ubi-K-mCherry-sfGFP::ura3	5, S13
YAnB65	Y8205	ura3::natMX-GDP^{pr}-Ubi-W-mCherry-sfGFP::ura3	5, S13
YAnB62	Y8205	ura3::natMX-GDP^{pr}-Ubi-N-mCherry-sfGFP::ura3	5, S13
YAnB64	Y8205	ura3::natMX-GDP^{pr}-Ubi-Q-mCherry-sfGFP::ura3	5, S13
YAnB66	Y8205	ura3::natMX-GDP^{pr}-Ubi-CL-mCherry-sfGFP::ura3	5, S13, S14
YAnB63	Y8205	ura3::natMX-GDP^{pr}-Ubi-P-mCherry-sfGFP::ura3	5, S13, S14, S16
YAnB67	Y8205	ura3::natMX-GDP^{pr}-Ubi-MH-(no degron)-mCherry-sfGFP::ura3	5, S12, S13
BY4741	–	MATa his3Δ1 leu2Δ0 met15Δ0 ura3Δ0	Ref[31]
–	BY4741	GLE1-TAP-HIS3MX	S3/Ref[9]
–	BY4741	GLE2-TAP-HIS3MX	S3/Ref[9]
–	BY4741	NDC1-TAP-HIS3MX	S3/Ref[9]
–	BY4741	POM152-TAP-HIS3MX	S3/Ref[9]
–	BY4741	NUP133-TAP-HIS3MX	S3/Ref[9]
–	BY4741	NUP145-TAP-HIS3MX	S3/Ref[9]
–	BY4741	NUP159-TAP-HIS3MX	S3/Ref[9]
–	BY4741	NUP84-TAP-HIS3MX	S3/Ref[9]
–	BY4741	NUP2-TAP-HIS3MX	S3/Ref[9]

Nature Biotechnology: doi:10.1038/nbt.2281

Name	Background	Description	used in Figure/Reference
AK951	ESM356-1	NDC1-sfGFP-mCherry-kanMX	S3
AK952	ESM356-1	NIC96-sfGFP-mCherry-kanMX	S3
AK953	ESM356-1	NUP133-sfGFP-mCherry-kanMX	S3
AK954	ESM356-1	NUP145-sfGFP-mCherry-kanMX	S3
AK1099	ESM356-1	NUP2-DsRed1-kanMX NIC96-eGFP-klTRP1	S5
yMaM234	ESM356-1	NUP2-DsRed1-kanMX ura3::NLS-eGFP::URA3 nup60Δ::natNT2	S5
UCC8650	S288c	MATa his3Δ1 leu2Δ0 lys2Δ0 ura3Δ0 hoΔ::SCW11^{pr}-Cre-EBD78-natMX	Ref[32]
yMaM244	UCC8650	NIC96-loxP-sfGFP-STOP-loxP-mCherry-kanMX	S6
yMaM113	ESM356-1	ura3::kanMX-GDP^{pr}-Ubi-Y-mCherry-sfGFP::ura3	S7, S11
yMaM112	ESM356-1	ura3::kanMX-GDP^{pr}-Ubi-R-mCherry-sfGFP::ura3	S7, S11
AK1154	ESM356-1	ura3::kanMX-GDP^{pr}-Ubi-A-mCherry-sfGFP::ura3	S7, S11
AK1155	ESM356-1	ura3::kanMX-GDP^{pr}-Ubi-C-mCherry-sfGFP::ura3	S7, S11
AK1156	ESM356-1	ura3::kanMX-GDP^{pr}-Ubi-D-mCherry-sfGFP::ura3	S7, S11
AK1157	ESM356-1	ura3::kanMX-GDP^{pr}-Ubi-E-mCherry-sfGFP::ura3	S7, S11
AK1158	ESM356-1	ura3::kanMX-GDP^{pr}-Ubi-G-mCherry-sfGFP::ura3	S7, S11
AK1159	ESM356-1	ura3::kanMX-GDP^{pr}-Ubi-H-mCherry-sfGFP::ura3	S7, S11
AK1160	ESM356-1	ura3::kanMX-GDP^{pr}-Ubi-K-mCherry-sfGFP::ura3	S7, S11
AK1161	ESM356-1	ura3::kanMX-GDP^{pr}-Ubi-L-mCherry-sfGFP::ura3	S7, S11
AK1162	ESM356-1	ura3::kanMX-GDP^{pr}-Ubi-N-mCherry-sfGFP::ura3	S7, S11
AK1163	ESM356-1	ura3::kanMX-GDP^{pr}-Ubi-P-mCherry-sfGFP::ura3	S7, S11
AK1164	ESM356-1	ura3::kanMX-GDP^{pr}-Ubi-Q-mCherry-sfGFP::ura3	S7, S11
AK1165	ESM356-1	ura3::kanMX-GDP^{pr}-Ubi-S-mCherry-sfGFP::ura3	S7, S11
AK1166	ESM356-1	ura3::kanMX-GDP^{pr}-Ubi-T-mCherry-sfGFP::ura3	S7, S11
AK1167	ESM356-1	ura3::kanMX-GDP^{pr}-Ubi-V-mCherry-sfGFP::ura3	S7, S11
AK1168	ESM356-1	ura3::kanMX-GDP^{pr}-Ubi-W-mCherry-sfGFP::ura3	S7, S11
AK1212	ESM356-1	ura3::natNT2-GAL1^{pr}-Ubi-M-RR-mCherry-sfGFP::ura3	S8
yMaM35	ESM356-1	p415-GDP^{pr}-Ubi-I-mCherry-sfGFP	S9
yMaM41	ESM356-1	p415-GDP^{pr}-Ubi-F-mCherry-sfGFP	S9
yMaM44	ESM356-1	p415-GDP^{pr}-Ubi-R-mCherry-sfGFP	S9
yMaM428	ESM356-1	p415-GDP^{pr}-Ubi-M-DsRed1-sfGFP	S9
yMaM429	ESM356-1	p415-GDP^{pr}-Ubi-I-DsRed1-sfGFP	S9
yMaM430	ESM356-1	p415-GDP^{pr}-Ubi-Y-DsRed1-sfGFP	S9
yMaM431	ESM356-1	p415-GDP^{pr}-Ubi-F-DsRed1-sfGFP	S9
yMaM432	ESM356-1	p415-GDP^{pr}-Ubi-R-DsRed1-sfGFP	S9
YAnB83	Y8205	ura3::natMX-GDP^{pr}-Ubi-CL-mCherry-SfGFP::ura3 cue1Δ::kanMX	S14
YAnB164	Y8205	ura3::natMX-GDP^{pr}-Ubi-CL-mCherry-sfGFP::ura3 ubc6Δ::kanMX	S14
YAnB141	Y8205	ura3::natMX-GDP^{pr}-Ubi-CL-mCherry-sfGFP::ura3 doa1Δ::kanMX	S14
YAnB142	Y8205	ura3::natMX-GDP^{pr}-Ubi-CL-mCherry-sfGFP::ura3 doa4Δ::kanMX	S14
YAnB81	Y8205	ura3::natMX-GDP^{pr}-Ubi-CL-mCherry-sfGFP::ura3 pre9Δ::kanMX	S14
YAnB82	Y8205	ura3::natMX-GDP^{pr}-Ubi-CL-mCherry-sfGFP::ura3 hul5Δ::kanMX	S14
YAnB117	Y8205	ura3::natMX-GDP^{pr}-Ubi-CL-mCherry-sfGFP::ura3 sem1Δ::kanMX	S14
YAnB161	Y8205	ura3::natMX-GDP^{pr}-Ubi-P-mCherry-SfGFP::ura3 ufd4Δ::hphNT1	S14, S16

Nature Biotechnology: doi:10.1038/nbt.2281

Name	Background	Description	used in Figure/Reference
YAnB95	Y8205	ura3::natMX-GDP^{pr}-Ubi-P-mCherry-sfGFP::ura3 pre9Δ::kanMX	S14
YAnB97	Y8205	ura3::natMX-GDP^{pr}-Ubi-P-mCherry-sfGFP::ura3 doa4Δ::kanMX	S14
YAnB104	Y8205	ura3::natMX-GDP^{pr}-Ubi-P-mCherry-sfGFP::ura3 doa1Δ::kanMX	S14
YAnB99	Y8205	ura3::natMX-GDP^{pr}-Ubi-P-mCherry-sfGFP::ura3 ubp6Δ::kanMX	S14
YAnB100	Y8205	ura3::natMX-GDP^{pr}-Ubi-P-mCherry-sfGFP::ura3 ubi4Δ::kanMX	S14
YAnB102	Y8205	ura3::natMX-GDP^{pr}-Ubi-P-mCherry-sfGFP::ura3 bro1Δ::kanMX	S14
YAnB103	Y8205	ura3::natMX-GDP^{pr}-Ubi-P-mCherry-sfGFP::ura3 sem1Δ::kanMX	S14
YAnB211	Y8205	ura3::natMX-GDP^{pr}-Ubi-P-mCherry -sfGFP::ura3 YEp195	S15
YAnB212	Y8205	ura3::natMX-GDP^{pr}-Ubi-P-mCherry -sfGFP::ura3 YEp195-CUP1pr-6His-Ubi	S15
YAnB213	Y8205	ura3::natMX-GDP^{pr}-Ubi-P-mCherry-sfGFP::ura3 ubp6Δ::kanMX YEp195	S15
YAnB214	Y8205	ura3::natMX-GDP^{pr}-Ubi-P-mCherry-sfGFP::ura3 ubp6Δ::kanMX YEp195-CUP1pr-6His-Ubi	S15
YAnB147	Y8205	ura3::natMX-GDP^{pr}-Ubi-P-mCherry-SfGFP::ura3 ubr1Δ::kanMX	S16
YAnB159	Y8205	ura3::natMX-GDP^{pr}-Ubi-P-mCherry-SfGFP::ura3 ubr1Δ::kanMX ufd4Δ::hphNT1	S16

Nature Biotechnology: doi:10.1038/nbt.2281

5.2 Supplementary Table 2

Plasmids used in this study.

Name	Backbone	Description	Reference
pYM-N19		natNT2-TEF promoter	Ref[33]
pFA6a-hphNT1			Ref[33]
pFA6a-natNT2			Ref[33]
pFA6a-kanMX			Ref[34]
pYM35	pFA6a-kanMX	pFA6a-DsRed1-kanMX	Ref[33]
pHM106-7	pFA6a-natNT2	pFA6a-eqFP611-natNT2	this study
pMaM134	pFA6a-hphNT1	pFA6a-DsRed1-hphNT1	this study
pMaM17	pFA6a-kanMX	pFA6a-mCherry-sfGFP-kanMX	this study
pMaM52	pFA6a-kanMX	pFA6a-sfGFP-mCherry-kanMX	this study
pMaM61	pFA6a-natNT2	pFA6a-mCherry-sfGFP-natNT2	this study
pMaM60	pFA6a-hphNT1	pFA6a-mCherry-sfGFP-hphNT1	this study
pMaM97	pYM-N19	pYM-N-natNT2-TEF-mCherry-sfGFP	this study
pMaM140	pFA6a-kanMX	pFA6a-loxP-sfGFP-STOP-loxP-mCherry-kanMX	this study
pRS306K		for linear integration into ura3 using kanMX selection	Ref[35]
p415-GDP		CEN ARS LEU2 with GDP promoter, CYC1 terminator	Ref[36]
p415-GAL1		CEN ARS LEU2 with GAL1 promoter, CYC1 terminator	Ref[36]
p415-TEF		CEN ARS LEU2 with TEF promoter, CYC1 terminator	Ref[36]
pKS88	pRS406	pRS406-pADH-NLS-2x-GFP	this study
pMaM99	p415-GDP	p415-GDP^{pr}-Ubi-M-mCherry-sfGFP	this study
pMaM98	p415-GDP	p415-GDP^{pr}-Ubi-I-mCherry-sfGFP	this study
pMaM103	p415-GDP	p415-GDP^{pr}-Ubi-Y-mCherry-sfGFP	this study
pMaM100	p415-GDP	p415-GDP^{pr}-Ubi-F-mCherry-sfGFP	this study
pMaM101	p415-GDP	p415-GDP^{pr}-Ubi-R-mCherry-sfGFP	this study
pMaM235	p415-GDP	p415-GDP^{pr}-Ubi-M-DsRed1-sfGFP	this study
pMaM236	p415-GDP	p415-GDP^{pr}-Ubi-I-DsRed1-sfGFP	this study
pMaM237	p415-GDP	p415-GDP^{pr}-Ubi-Y-DsRed1-sfGFP	this study
pMaM238	p415-GDP	p415-GDP^{pr}-Ubi-F-DsRed1-sfGFP	this study
pMaM239	p415-GDP	p415-GDP^{pr}-Ubi-R-DsRed1-sfGFP	this study
pMaM104	pMaM99	p415-TEF^{pr}-Ubi-M-mCherry-sfGFP	this study
pMaM105	pMaM103	p415-TEF^{pr}-Ubi-Y-mCherry-sfGFP	this study
pMaM106	pMaM99	p415-GAL1^{pr}-Ubi-M-mCherry-sfGFP	this study
pMaM109	pMaM103	p415-GAL1^{pr}-Ubi-Y-mCherry-sfGFP	this study
pMaM46	pRS306K	pRS306K-GDP^{pr}-Ubi-M-mCherry-sfGFP	this study
pMaM47	pRS306K	pRS306K-GDP^{pr}-Ubi-I-mCherry-sfGFP	this study
pMaM48	pRS306K	pRS306K-GDP^{pr}-Ubi-F-mCherry-sfGFP	this study
pMaM66	pRS306K	pRS306K-GDP^{pr}-Ubi-R-mCherry-sfGFP	this study
pMaM67	pRS306K	pRS306K-GDP^{pr}-Ubi-Y-mCherry-sfGFP	this study
pAK146	pRS306K	pRS306K-GDP^{pr}-Ubi-A-mCherry-sfGFP	this study

Nature Biotechnology: doi:10.1038/nbt.2281

Name	Backbone	Description	Reference
pAK147	pRS306K	pRS306K-GDP^{pr}-Ubi-C-mCherry-sfGFP	this study
pAK148	pRS306K	pRS306K-GDP^{pr}-Ubi-D-mCherry-sfGFP	this study
pAK149	pRS306K	pRS306K-GDP^{pr}-Ubi-E-mCherry-sfGFP	this study
pAK150	pRS306K	pRS306K-GDP^{pr}-Ubi-G-mCherry-sfGFP	this study
pAK151	pRS306K	pRS306K-GDP^{pr}-Ubi-H-mCherry-sfGFP	this study
pAK152	pRS306K	pRS306K-GDP^{pr}-Ubi-K-mCherry-sfGFP	this study
pAK153	pRS306K	pRS306K-GDP^{pr}-Ubi-L-mCherry-sfGFP	this study
pAK154	pRS306K	pRS306K-GDP^{pr}-Ubi-N-mCherry-sfGFP	this study
pAK155	pRS306K	pRS306K-GDP^{pr}-Ubi-P-mCherry-sfGFP	this study
pAK156	pRS306K	pRS306K-GDP^{pr}-Ubi-Q-mCherry-sfGFP	this study
pAK157	pRS306K	pRS306K-GDP^{pr}-Ubi-S-mCherry-sfGFP	this study
pAK158	pRS306K	pRS306K-GDP^{pr}-Ubi-T-mCherry-sfGFP	this study
pAK159	pRS306K	pRS306K-GDP^{pr}-Ubi-V-mCherry-sfGFP	this study
pAK160	pRS306K	pRS306K-GDP^{pr}-Ubi-W-mCherry-sfGFP	this study
pJLM1	pRS306K	pRS306K-GDP^{pr}-Ubi-CL-mCherry-sfGFP	this study
pMaM209	pRS306K	pRS306K-GDP^{pr}-Ubi-M-RR-mCherry-sfGFP	this study
pMaM207		pETM-11-6xHis-TEV-sfGFP	this study
pMaM208		pETM-11-6xHis-TEV-mCherry-sfGFP	this study
YEp195		2µ URA3	
YEp195-CUP1^{pr}-6xHis-ubiquitin	YEp195	YEp195-CUP1^{pr}-6xHis-ubiquitin	

5.3 Supplementary Table 3

Results of the screens for components of the N-end rule pathway.

This table is provided as an .xls (Excel) file, with each screen in a separate spreadsheet named X(Z) according to the variable residues in the corresponding Ubi-X(Z)-mCherry-sfGFP construct. Only gene deletions with positive Δ-scores in both the sfGFP and mCherry/sfGFP channels are listed and ranked by the median d of the three screen replicates (see Online Methods).

Nature Biotechnology: doi:10.1038/nbt.2281

6 Supplementary Movies

6.1 Supplementary Movie 1

Movie corresponding to Figure 3d (i, ii). Maximum projections of deconvolved stacks (3 planes with 1 µm separation) are shown, with Nup2-DsRed1 in red and NLS-eGFP in green. Scale bar: 5 µm.

6.2 Supplementary Movie 2

Movie corresponding to Figure 3d (iii). Single plane deconvolved images are shown, with Nup2-DsRed1 in red and NLS-eGFP in green. Scale bar: 5 µm.

Nature Biotechnology: doi:10.1038/nbt.2281

7 Supplementary References

1. Wachsmuth, M., Waldeck, W. & Langowski, J. Anomalous diffusion of fluorescent probes inside living cell nuclei investigated by spatially-resolved fluorescence correlation spectroscopy. *J. Mol. Biol.* **298**, 677–689 (2000).
2. Subach, F. V. *et al.* Monomeric fluorescent timers that change color from blue to red report on cellular trafficking. *Nat. Chem. Biol.* **5**, 118–126 (2009).
3. Newman, J. R. S. *et al.* Single-cell proteomic analysis of S. cerevisiae reveals the architecture of biological noise. *Nature* **441**, 840–846 (2006).
4. Winey, M., Yarar, D., Giddings, T. H. & Mastronarde, D. N. Nuclear pore complex number and distribution throughout the Saccharomyces cerevisiae cell cycle by three-dimensional reconstruction from electron micrographs of nuclear envelopes. *Mol. Biol. Cell* **8**, 2119–2132 (1997).
5. Khmelinskii, A., Keller, P. J., Lorenz, H., Schiebel, E. & Knop, M. Segregation of yeast nuclear pores. *Nature* **466**, E1 (2010).
6. Förster, T. Zwischenmolekulare energiewanderung und fluoreszenz. *Annalen der Physik* (1948).
7. Belle, A., Tanay, A., Bitincka, L., Shamir, R. & O'Shea, E. K. Quantification of protein half-lives in the budding yeast proteome. *Proc. Natl. Acad. Sci. U.S.A.* **103**, 13004–13009 (2006).
8. Huh, W.-K. *et al.* Global analysis of protein localization in budding yeast. *Nature* **425**, 686–691 (2003).
9. Ghaemmaghami, S. *et al.* Global analysis of protein expression in yeast. *Nature* **425**, 737–741 (2003).
10. Storici, F. & Resnick, M. A. The delitto perfetto approach to in vivo site-directed mutagenesis and chromosome rearrangements with synthetic oligonucleotides in yeast. *Meth. Enzymol.* **409**, 329–345 (2006).
11. Varshavsky, A. The N-end rule pathway and regulation by proteolysis. *Protein Sci.* **20**, 1298–1345 (2011).
12. Loewen, C. J. R. & Levine, T. P. A highly conserved binding site in vesicle-associated membrane protein-associated protein (VAP) for the FFAT motif of lipid-binding proteins. *J. Biol. Chem.* **280**, 14097–14104 (2005).
13. Rebollo, E. *et al.* Functionally unequal centrosomes drive spindle orientation in asymmetrically dividing Drosophila neural stem cells. *Dev. Cell* **12**, 467–474 (2007).
14. Pédelacq, J.-D., Cabantous, S., Tran, T., Terwilliger, T. C. & Waldo, G. S. Engineering and characterization of a superfolder green fluorescent protein. *Nat. Biotechnol.* **24**, 79–88 (2006).
15. Shaner, N. C. *et al.* Improved monomeric red, orange and yellow fluorescent proteins derived from Discosoma sp. red fluorescent protein. *Nat. Biotechnol.* **22**, 1567–1572 (2004).
16. Barlowe, C. *et al.* COPII: a membrane coat formed by Sec proteins that drive vesicle budding from the endoplasmic reticulum. *Cell* **77**, 895–907 (1994).
17. Siniossoglou, S. *et al.* A novel complex of nucleoporins, which includes Sec13p and a Sec13p homolog, is essential for normal nuclear pores. *Cell* **84**, 265–275 (1996).
18. Knop, M. *et al.* Epitope tagging of yeast genes using a PCR-based strategy: more tags and improved practical routines. *Yeast* **15**, 963–972 (1999).
19. Frey, S., Pool, M. & Seedorf, M. Scp160p, an RNA-binding, polysome-associated protein, localizes to the endoplasmic reticulum of Saccharomyces cerevisiae in a microtubule-dependent manner. *J. Biol. Chem.* **276**, 15905–15912 (2001).
20. Gross, L. A., Baird, G. S., Hoffman, R. C., Baldridge, K. K. & Tsien, R. Y. The structure of the chromophore within DsRed, a red fluorescent protein from coral. *Proc. Natl. Acad. Sci. U.S.A.* **97**, 11990–11995 (2000).
21. Kenna, M. A., Petranka, J. G., Reilly, J. L. & Davis, L. I. Yeast N1e3p/Nup170p is required for normal stoichiometry of FG nucleoporins within the nuclear pore complex. *Molecular and Cellular Biology* **16**, 2025–2036 (1996).

Nature Biotechnology: doi:10.1038/nbt.2281

22. Dilworth, D. J. *et al.* Nup2p dynamically associates with the distal regions of the yeast nuclear pore complex. *J. Cell Biol.* **153**, 1465–1478 (2001).
23. Verzijlbergen, K. F. *et al.* Recombination-induced tag exchange to track old and new proteins. *Proc. Natl. Acad. Sci. U.S.A.* **107**, 64–68 (2010).
24. Heun, P., Laroche, T., Shimada, K., Furrer, P. & Gasser, S. M. Chromosome dynamics in the yeast interphase nucleus. *Science* **294**, 2181–2186 (2001).
25. Bachmair, A., Finley, D. & Varshavsky, A. In vivo half-life of a protein is a function of its amino-terminal residue. *Science* **234**, 179–186 (1986).
26. Bachmair, A. & Varshavsky, A. The degradation signal in a short-lived protein. *Cell* **56**, 1019–1032 (1989).
27. Johnson, E. S., Ma, P. C., Ota, I. M. & Varshavsky, A. A proteolytic pathway that recognizes ubiquitin as a degradation signal. *J. Biol. Chem.* **270**, 17442–17456 (1995).
28. Clute, P. & Pines, J. Temporal and spatial control of cyclin B1 destruction in metaphase. *Nat. Cell Biol.* **1**, 82–87 (1999).
29. Hwang, C.-S., Shemorry, A., Auerbach, D. & Varshavsky, A. The N-end rule pathway is mediated by a complex of the RING-type Ubr1 and HECT-type Ufd4 ubiquitin ligases. *Nat. Cell Biol.* **12**, 1177–1185 (2010).
30. Tong, A. H. Y. & Boone, C. High-Throughput Strain Construction and Systematic Synthetic Lethal Screening in Saccharomyces cerevisiae. *Meth. Microbiol.* **36**, 369–386 (2007).
31. Brachmann, C. B. *et al.* Designer deletion strains derived from Saccharomyces cerevisiae S288C: a useful set of strains and plasmids for PCR-mediated gene disruption and other applications. *Yeast* **14**, 115–132 (1998).
32. Lindstrom, D. L. & Gottschling, D. E. The mother enrichment program: a genetic system for facile replicative life span analysis in Saccharomyces cerevisiae. *Genetics* **183**, 413–422 (2009).
33. Janke, C. *et al.* A versatile toolbox for PCR-based tagging of yeast genes: new fluorescent proteins, more markers and promoter substitution cassettes. *Yeast* **21**, 947–962 (2004).
34. Wach, A., Brachat, A., Pöhlmann, R. & Philippsen, P. New heterologous modules for classical or PCR-based gene disruptions in Saccharomyces cerevisiae. *Yeast* **10**, 1793–1808 (1994).
35. Taxis, C. & Knop, M. System of centromeric, episomal, and integrative vectors based on drug resistance markers for Saccharomyces cerevisiae. *BioTechniques* **40**, 73–78 (2006).
36. Mumberg, D., Müller, R. & Funk, M. Yeast vectors for the controlled expression of heterologous proteins in different genetic backgrounds. *Gene* **156**, 119–122 (1995).

Nature Biotechnology: doi:10.1038/nbt.2281